Twist and Degrade – Impact of Molecular Structure on the Photostability of Non-Fullerene Acceptors and Their Photovoltaic Blends

Joel Luke[a], Emily M. Speller[b], Andrew Wadsworth[c], Mark F. Wyatt[d], Stoichko Dimitrov[b], Zhe Li[e], Wing C. Tsoi[b], Iain McCulloch[c,f], Diego Bagnis[g], James R. Durrant[b, c], Ji-Seon Kim[a]*

(a) Department of Physics and Centre for Plastic Electronics, Imperial College London, London, SW7 2AZ, UK. E-mail: ji-seon.kim@imperial.ac.uk

(b) SPECIFIC IKC, College of Engineering, Swansea University, Bay Campus, Fabian Way, Swansea, Wales, SA1 8EN, UK

(c) Department of Chemistry and Centre for Plastic Electronics, Imperial College London, London, SW7 2AY, UK

(d) EPSRC UK National Mass Spectrometry Facility (NMSF), Swansea University Medical School, Singleton Park, Swansea SA2 8PP, UK

(e) School of Engineering, Cardiff University, CF24 3AA, UK

(f) KSC King Abdullah University of Science and Technology, Thuwal, 23955-6900, Saudi Arabia

(g) Centro de Inovações, CSEM BRASIL, Av. José Cândido da Silveira, 2000 - Horto Florestal, Belo Horizonte - MG, 31035-536

Keywords: organic solar cells; non-fullerene acceptors (NFA); photo-stability; NFA molecular structures; conformational change

Non-fullerene acceptors (NFAs) dominate organic photovoltaic (OPV) research due to their promising efficiencies and stabilities. However, there is very little investigation into the molecular processes of degradation, which is critical to guiding design of novel NFAs for long-lived, commercially viable OPVs. Here we investigate the important role of

molecular structure and conformation on NFA photostability in air by comparing structurally similar but conformationally different promising NFAs; planar O-IDTBR and non-planar O-IDFBR. We identify a three-phase degradation process: (i) initial photo-induced conformational change (i.e. torsion about the Core-BT dihedral), induced by non-covalent interactions with environmental molecules, (ii) followed by photo-oxidation and fragmentation, leading to chromophore bleaching and degradation product formation, and (iii) finally complete chromophore bleaching. Initial conformational change is a critical prerequisite for further degradation, providing fundamental understanding of the relative stability of IDTBR and IDFBR, where the already-twisted IDFBR is more prone to degradation. When blended with the donor polymer P3HT, both NFAs exhibit improved photostability whilst the photostability of the polymer itself is significantly reduced by the more miscible twisted NFA. Our findings elucidate the important role of NFA molecular structure on photostability of OPV systems, and provide vital insights into molecular design rules for intrinsically photostable NFAs.

1. Introduction

Organic photovoltaics (OPVs) have received large amounts of interest in research and commercial development due to their potential for low-cost, solution processable, flexible solar cells. Solution processed OPV devices are based on an organic bulk heterojunction (BHJ) blend consisting of a conjugated donor polymer and a small molecule acceptor. Typically the small molecules used have been fullerene derivatives such as $PC_{60}BM$, $PC_{70}BM$ and ICBA, achieving efficiencies of 11%[1,2] and lifetimes exceeding several years[3].

However, progress in fullerene based devices have stalled due to several intrinsic limitations of fullerene based derivatives. An inability to tune the chemical structure inhibits morphological or energetic optimisation, to the effect that progress in the field has mostly been

driven by the design and fine tuning of the donor polymers used within the blends.[4] Fullerenes are also poor absorbers possessing a wide band gap which limits their contribution to light harvesting across the entire solar spectrum. Stability issues are also common, with light induced effects causing strong burn-in degradation[5,6], poor thermal stability[7–9] and photo-oxidation[10,11] reducing the viability of using fullerene-based acceptors in commercial modules. Efforts have been made to address these issues and improvements in stability have been achieved but morphological and light-induced degradation effects still remain. In the last few years NFAs have replaced fullerenes as the acceptor of choice and have already achieved high efficiencies > 13 %[12,13] and burn-in free devices[14,15]. Accompanied by reports of good compatibility with non-chlorinated solvents[16] and low thickness dependent performance[17] NFAs provide encouraging potential for commercial scale-up. However, the origin of these impressive stabilities is poorly understood, and there is still plenty of room for improvement, especially concerning their stability in air.

Due to the different classes of molecules used as NFAs it is difficult to apply broad design rules. For example, it is known that there is a need to balance an acceptors propensity to crystallise with its miscibility in the donor polymer, to achieve an optimal BHJ morphology. One approach, demonstrated by Hwang *et al*, is to disrupt the packing of NDI-based dimers by increasing the torsion angle between the two units, leading to an improved morphology and better device performance.[18] Another approach to achieve an optimal morphology, taken by Holliday *et al*, is to increase the planarity and therefore crystallinity of rod-like A-D-A acceptors, which are otherwise too miscible with the polymer.[19,20] These examples highlight the importance of NFA molecular structure on OPV device performance, but also emphasize the difficulty in defining universal design rules for these different classes of molecule.

In this work we are concerned with the most successful class of NFAs, which are those based on linear A-D-A architectures such as IDTBR[20,21], ITIC[17,18] and their derivatives[24].

IDTBR is composed of an electron-rich indacenodithiophene (IDT) unit with *n*-octyl side chains, flanked by the electron withdrawing units: benzothiadiazidole (BT) and 3-ethyl-rhodanine (**Figure 1c**). It has shown promising photo and morphological stability and high performance with the semi-crystalline homo-polymer poly(3-hexylthiophene) (P3HT) achieving an power conversion efficiency (PCE) of 7 %.[25] P3HT has often been used as a model system for studying organic solar cells[26], and is still relevant for use in inexpensive large-scale modules due to it being readily available and relatively lower cost compared to other higher efficiency state-of-the-art donor-acceptor polymers. The best performing P3HT /NFA device is realised when a third component, the acceptor IDFBR, is added in a ternary blend[21]. IDFBR is analogous to IDTBR but with an indenofluorene (IDF) core replacing IDT (Figure 1d).

Due to the different core units the two acceptors adopt different molecular conformations as elucidated from single crystal structure determination and density functional theory simulations (Fig 1c and 1d) and reported in the literature.[20,21] IDTBR shows a planar backbone whilst IDFBR, due to steric clash between adjacent ortho-hydrogen atoms on the IDF and BT units, adopts a more twisted conformation with a dihedral angle of 33°. In this study, we investigate in detail how this minor change in chemical structure can cause significant changes in photostability, and then how this affects BHJ blend stability. For this, we employ P3HT as a model system to investigate the interaction of donor and acceptor and how this effects photostability in air. By elucidating the molecular origin of photostability we provide guidance for the design of NFAs that avoid undesirable degradation pathways and create intrinsically stable photoactive BHJ layers which are resistant to the ingress of oxygen and moisture removing the need for encapsulation, which is often one of the more costly components of module fabrication.

In order to explore active layer degradation and stability we utilize complementary spectroscopic techniques supported by quantum chemical simulations and structural probes. We also employ *in situ* Raman spectroscopy studies that enable us to track both vibrational and luminescence changes. This is important because in organic semiconductors, electronic excitations and molecular vibrations are strongly coupled due to distortion of the conjugated molecular backbone when in the excited or charged state. By measuring simultaneously the luminescence and vibrational transitions of the molecules, it is therefore possible to gain information about the conformation of molecules and the emission property of organic films. In particular, under resonant excitation conditions (when the energy of the excitation photon matches the energy of a dipole-allowed electronic transition of the molecule), a strong enhancement in the Raman scattering intensity as well as photoluminescence occur. Resonant Raman spectroscopy is highly sensitive to the molecular structure and conformation of π-conjugated molecules[27,28] and has been used previously to investigate the morphology[26] and stability of several bulk heterojunction OPV blends.[29–31]

We find that IDFBR is substantially less photostable than IDTBR in both nitrogen and air. By using *in situ* resonant Raman spectroscopy we propose a three-phase degradation mechanism that explains this difference. The first step is a photo-induced conformational change, namely an increase in the dihedral angle between the core and BT units. This leads to the second step of degradation, likely fragmentation or photo-oxidation, before reaching the third phase in which the chromophore is bleached completely. IDFBR, due to its more twisted backbone is already prone to the second step of degradation, resulting in rapid photo-degradation in both nitrogen and air.

Upon blending with P3HT, the two acceptors form different morphologies as observed previously. IDFBR is found to be more miscible with the polymer, whilst IDTBR forms a fairly well phase-separated morphology with P3HT. The photostability of the blend is also

investigated, with both NFAs being stabilised by blending. On the other hand, P3HT degradation is accelerated by blending with twisted IDFBR, but when blended with planar IDTBR the polymer retains a similar stability to the neat films. The degradation of P3HT is found to go via a chemical oxidation which produces signatures that are similar to doping. This study highlights the importance of molecular design on NFA stability, and we propose that planarity and rigidity should be taken into account when designing stable acceptors. We also show how NFAs impact on the polymer stability in the photoactive layer blend, and suggest possible mechanisms for this.

2. Results and Discussion

2.1 Neat film morphology

To enable discussions on photostability and BHJ blends of the materials, we firstly discuss the neat film morphology and effect of annealing of NFAs.

Figure 1a shows the absorption spectra of as-cast IDTBR and IDFBR films. Both acceptors show two prominent absorption peaks within the visible range. The lower energy peak, arising from the HOMO→LUMO transition, is significantly red-shifted for IDTBR, which is due to its more electron rich core, raising the HOMO energy level, as well as a more planar molecular structure, as elucidated by DFT simulations (Figure 1b). This planar structure enables effective π-stacking in the solid state, resulting in a more crystalline morphology than IDFBR.[20,21] For both molecules the HOMO is delocalised along the main conjugated backbone with most electron density sitting on the electron rich core, whilst the LUMO is partially localised to the BT unit (**Figure S1**). Due to the planarity of IDTBR, its HOMO and LUMO wavefunctions are more delocalised resulting in a large overlap between them, thereby enhancing oscillator strength of this transition. As opposed to IDTBR, the more twisted IDFBR (Figure 1c) has more localised HOMO and LUMO wavefunctions, resulting in stronger CT-like character, as seen by the broad, less vibronic structure and a more typical symmetrical camel-back absorption associated with CT-like transitions in D-A organic molecules.[30]

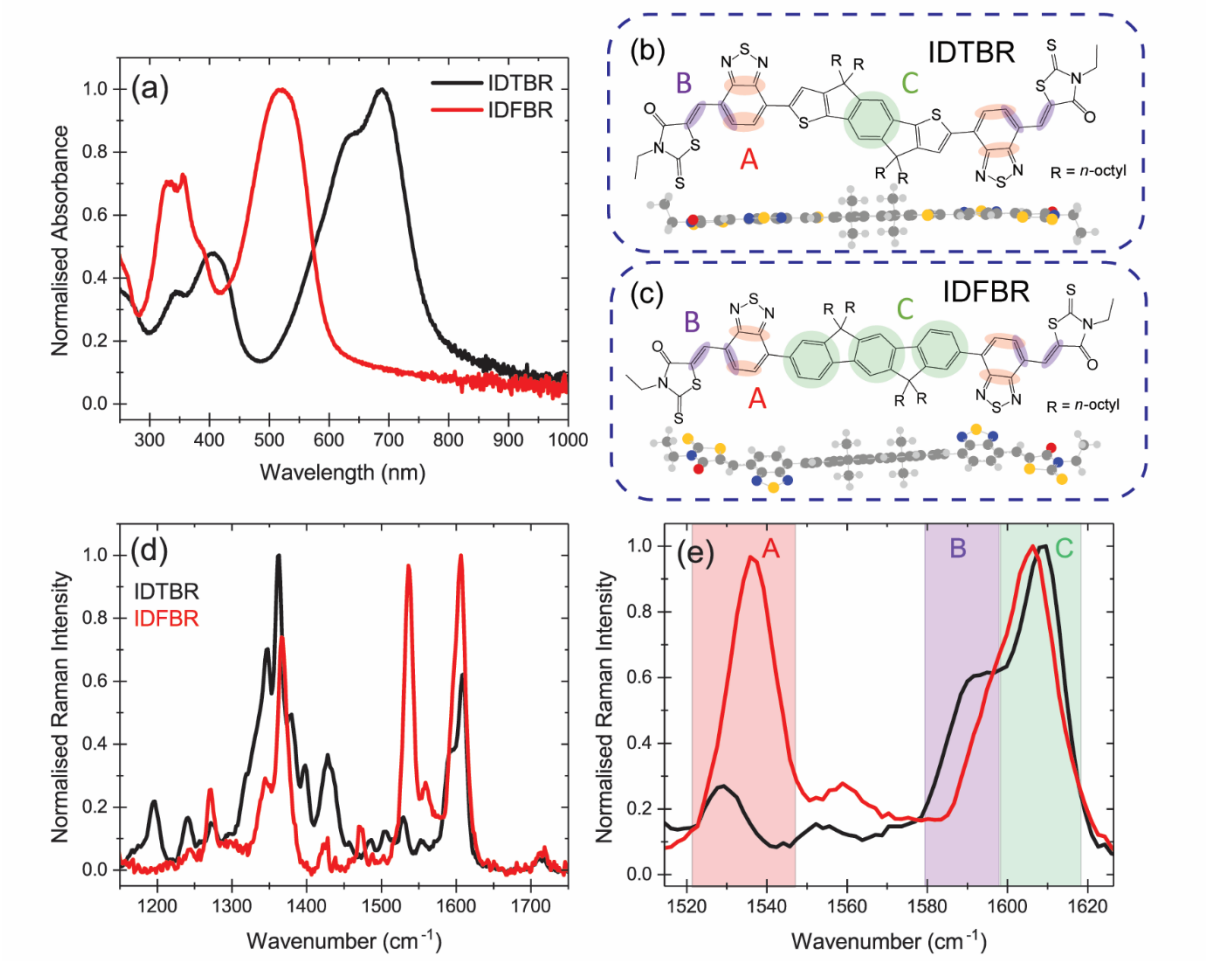

Figure 1. (a) UV-vis absorption spectra of as-cast thin films of IDTBR and IDFBR. Chemical structure with vibrational mode assignment and DFT optimised structure of IDTBR (b) and IDFBR (c). (d) Normalised Raman spectra of as-cast films of IDTBR and IDFBR at 457 nm excitation, the highlighted region is the region shown in (e). (e) Normalised and assigned Raman spectra of IDTBR (black) and IDFBR (red dash) normalised to the phenyl mode, here labelled C.

Figure 1d shows the normalised Raman spectra of IDTBR and IDFBR, at 457 nm excitation. There are common peaks between the two spectra: a carbonyl peak at ~1710 cm^{-1} arises from the rhodanine groups, the peak at ~1600 cm^{-1} is assigned to the fused phenyl groups in the core of both molecules and BT peaks are found at ~1530 cm^{-1} and ~1350 cm^{-1}. The phenyl peak of IDFBR has a much larger relative intensity due to there being three phenyl rings in the IDF core, compared to just the one in IDTBR. There are also clear differences between the spectra arising from the thiophene peaks present (1380-1450 cm^{-1}) for IDTBR which are not observed for IDFBR. A full spectral assignment of these spectra is given in **Figure S2**. Figure 1e shows the assignment of 3 key peaks, with the corresponding bonds highlighted in Figure 1b and 1c. Peak A, centred at 1529 cm^{-1} for IDTBR, is localised to the BT unit of

the acceptor and is assigned to the symmetric stretch of the C-C bonds within the benzene ring. Peak B, at 1592 cm^{-1} is assigned to the alkene bond between the BT and rhodanine units, and peak C, at 1609 cm^{-1}, is a vibration localised to the phenyl rings within the core IDT unit. IDFBR has equivalent A and C peaks at 1536 and 1606 cm^{-1} with peak B appearing as a low frequency shoulder of peak C at 1595cm^{-1}. Peak assignment has been guided by DFT simulations, and comparison with the literature.[32,33] For a full description of the morphology changes upon annealing of these films please see **Figure S3**.

2.2 Neat film photostability

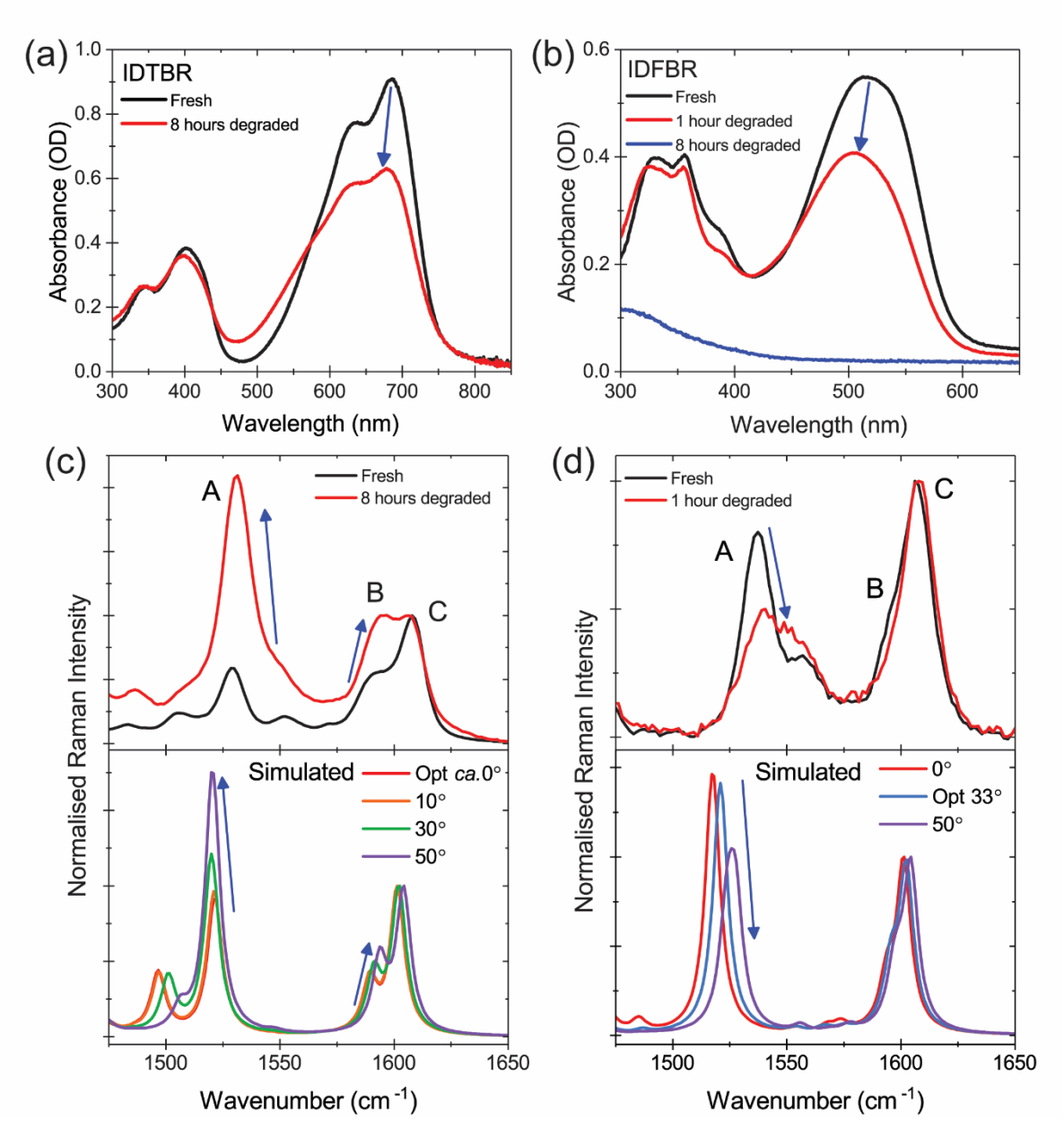

Figure 2. (a+b) Absorption spectra of fresh and degraded as-cast films of IDTBR (a) and IDFBR (b). (c+d) Top, normalised Raman spectra of IDTBR at 488 nm excitation (c) and IDFBR at 457 nm excitation (d) of fresh and degraded as-cast films,

with vibrational peak assignment consistent with Figure 1. Bottom, normalised DFT simulated Raman spectra of IDTBR (c) and IDFBR (d) at various core-BT dihedral angles. The chemical structures show the dihedral angle in question. The optimised angle for IDTBR is ~0° whilst IDFBR is ~33°.

The absorption spectra of fresh and degraded as-cast neat films of the two acceptors are shown in **Figure 2a and 2b**. Degradation has been carried out using a solar simulator at 1 sun illumination within a temperature controlled environment in air. After 8 hours of illumination there is a bleaching and slight blue-shift of the lower energy peak of IDTBR. Similarly the low energy transition of IDFBR shows the same bleaching and blue-shift but this is apparent after just 1 hour of illumination. After an equivalent 8 hours of illumination there is a near complete bleaching of absorption within the visible range, indicating that the more amorphous, twisted IDFBR is much less photostable in air than the planar, crystalline IDTBR.

The normalised Raman spectra of fresh and degraded acceptors are shown in Figure 2c and 2d. After 8 hours of illumination IDTBR shows an increase in relative intensity of peak A and B with respect to peak C. To investigate the origin of these spectral changes, Raman spectra of IDTBR at different IDT-BT torsion angles were simulated. It was found that increasing the IDT-BT dihedral angle resulted in spectral changes consistent with those observed experimentally. Similarly, IDFBR also shows changes in the relative peak intensity of Peak A upon degradation, but the opposite change is observed, which might indicate different packing and orientation of BT units in IDFBR thin films. After 1 hour of illumination IDFBR already shows a 41% decrease in the relative intensity of peak A, with respect to peak C, which itself shifts 2 cm^{-1} to higher frequencies. DFT calculations confirm that these peak changes are again consistent with a higher torsion between the IDF and BT units inducing a more twisted structure. These observations suggest that illumination of both of these NFAs in air induces the same molecular conformational change, namely a rotation about the core-BT dihedral. Such changes in BT relative peak intensity (peak A) and phenyl peak shift (peak C) has previously been correlated to a decrease in backbone planarity for the polymer F8BT by Schmidtke *et al*.[32]

The bleaching of absorption observed in the lower energy transition for the as-cast films can be understood by this molecular conformational change. The CT-like character of this low energy

transition has been described by Jespersen *et al.* for conjugated polymers containing BT units.[34] IDFBR with its more twisted molecular structure has more of this CT-like behaviour, with the HOMO and LUMO being more spatially confined to the donor and acceptor units respectively. In contrast, the HOMO and LUMO of IDTBR, due to its planar structure, are more delocalised along the entire molecule, but still retains some CT character. This more delocalised transition has a higher oscillator strength, due to increased orbital overlap (Figure 3c, d). It is consistent with the study by Vezie *et al.*, who show that a longer polymer persistence length, which is correlated to planarity, is needed for a higher optical density.[35] If upon continuous light illumination and degradation there is a twisting about the donor-acceptor dihedral angle, it will cause more localisation of the HOMO and LUMO wavefunctions to the donor and acceptor units respectively, reducing the transition oscillator strength thus quenching the lowest energy absorption transition, as observed. The observed blue-shift of both IDTBR and IDFBR is due to the decreased effective conjugation length of the twisted molecules. Simulated UV/vis spectra for the planar and twisted non-fullerene acceptors support this hypothesis, showing that the lower energy transition is bleached and blue-shifted upon increasing the Core-BT torsion angle (**Figure S4**).

We note that the higher energy peak remains relatively unchanged during degradation, whilst the lower energy CT-like absorption which involves the BT unit, is selectively quenched in both molecules. This selective degradation of the lower energy absorption can be related to much stronger absorption of low energy photons (<450 nm) in both molecules (**Figure S5**), but also more importantly to its CT-like character involving the BT unit, which we have shown is responsible for degradation. Interestingly the more significant bleaching of the lower energy absorption transition is observed in IDFBR, which may originate from the higher energy photons (450-600 nm) involved in this transition than IDTBR (500-750 nm), as reported for blue-OLEDs.[36,37]

To further investigate the chemical processes undertaken by these materials under illumination in air, mass spectroscopy was conducted to probe for degradation products. After 1 hour of degradation, IDFBR shows clear molecular fragmentation which becomes more pronounced after 8 hours of degradation (**Figure S6**). This is consistent with the near complete bleaching of absorption seen for the

8 hour degraded IDFBR film. The PL spectrum of fresh IDFBR shows an emission at 650 nm, whilst the 8 hour degraded film shows only a blue-shifted emission at 550 nm (**Figure S7**), which we assign to emission from the observed fragmentation products which are assumed to have a reduced effective conjugation length and therefore higher optical band gap. Fragmentation is clearly occurring within the IDFBR film, alongside the conformational change suggested above.

The mass spectrum of IDTBR after 8 hours of illumination in air (Figure S6) shows significantly less fragmentation but interestingly, there are small peaks appearing at 1340 and 1356 m/z, which are 16 and 32 m/z units above the molecular ion peak at 1324, indicating the addition of oxygen to the structure, suggesting chemical oxidation has occurred. Due to the small signatures of oxidation and fragmentation in degraded IDTBR it is concluded that although these processes are occurring, they are minor processes which cannot account for the large Raman changes observed upon degradation.

So far the discussion has been concerned with as-cast films. As described in the supporting discussion (Figure S3), for IDFBR, thermal annealing is shown to make no difference to the molecular conformation or morphology, and its photostability is not significantly affected. On the other hand, IDTBR is shown to increase in crystallinity upon thermal annealing which stabilises the film towards photo-degradation in air (**Figure S8**). This is observed as a reduction in the bleaching of absorption after the same degradation time as the as-cast films. Raman spectra of the annealed IDTBR show the same changes seen in the as-cast films, but are less pronounced, indicating that the same degradation mechanism is occurring, albeit at a slower rate.

2.3 *In situ* degradation

In situ degradation using the laser excitation as an accelerated degradation source was carried out to further investigate the photo-degradation processes of these acceptors. Using the Raman experimental set-up it is possible to track Raman peaks and PL as a function of laser illumination time.

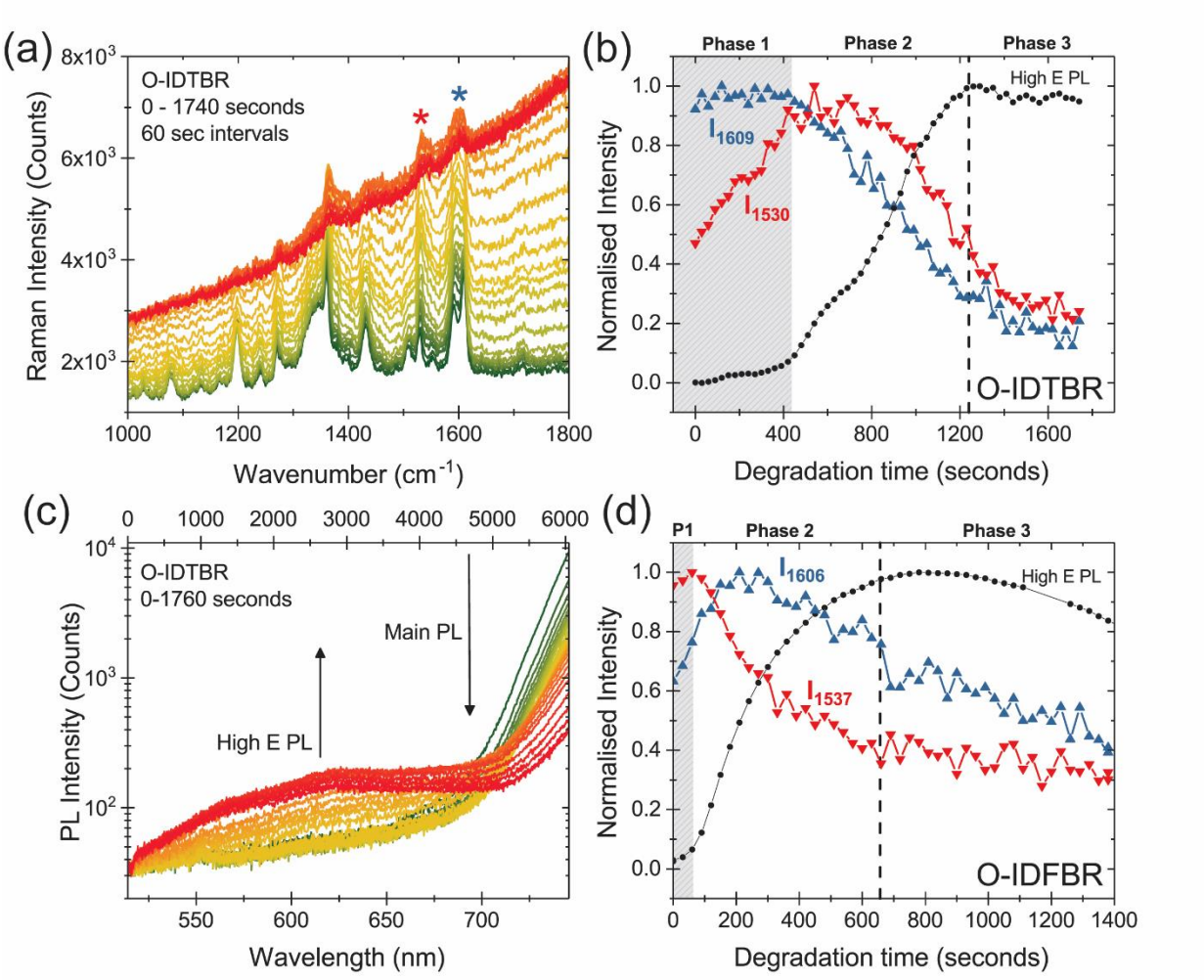

Figure 3. (a) Raw in situ Raman spectra at 457 nm excitation of a neat, annealed IDTBR film shown as a function of laser illumination time starting with green spectra and progressing to red, the red and blue stars indicate the positions of the vibrational modes labelled A and C in Figure 1. 4(b) Normalised data extracted from (a) including intensities of peaks A and C (red and blue lines) and the increase in background PL (filled black circles). (c) In situ PL spectra of the same IDTBR film taken at 514 nm excitation as a function of laser illumination time. (d) Extracted information from in situ Raman spectra of a neat IDFBR film using 457 nm laser probe taken at increasing laser illumination time. It should be noted that plots (b) and (d) show the absolute peak intensities after PL background removal, these values are then normalised to allow for concurrent plotting.

Figure 3a shows the raw Raman spectra obtained during accelerated (see Experimental) *in situ* degradation of annealed IDTBR. With increasing illumination time there is a delayed increase in the background (caused by increasing PL), a change in the relative peak intensities, and towards longer times a reduction in Raman peak intensity of all peaks. For a more in depth analysis of these spectra, the peak intensities of the BT and phenyl peaks (starred) and the PL background are extracted and

summarised in Figure 3b. We observe three distinct phases in the degradation process. Phase 1 (0 - 400 seconds), is predominantly characterised by the molecular conformational change, namely the rotation about the IDT-BT dihedral, as observed in the solar simulator degraded samples. The Raman intensity of the BT peak (A) at 1530 cm^{-1} increases to a maximum, whilst the intensity of the phenyl peak (C) at 1609 cm^{-1} and PL background remain constant, indicating no loss of the chromophore. Figure 4c shows that the main emission from the $S_1 \rightarrow S_0$ transition (> 700 nm) is quickly quenched during this first phase of degradation, which is consistent with the PL quenching observed in the solar simulator degraded samples (Figure S7). Phase 2 (400-1200 seconds) is defined as the point at which the background PL in Figure 4a begins to increase, whilst the Raman intensity of the 1609 and 1530 cm^{-1} peaks begins to be quenched. This increase in background PL is due to the appearance of a new distinct high energy PL peak at *ca.*625 nm, which is orders of magnitude weaker than the initial $S_1 \rightarrow S_0$ emission. This quenching of the IDTBR vibrational modes and appearance of the new high energy PL peak suggest a strong change to the chromophore of the molecule upon continuous illumination. Phase 3 (>1200 seconds) begins when the high energy PL has reached a maximum with no more degradation product forming after this point. The Raman peak intensities of the initial molecule are now negligible, indicating that the IDTBR molecules are heavily degraded, and the initial chromophore has been almost completely bleached. If degradation were continued (not shown here) this product PL begins to decrease, relating to breakdown of the degradation product. Phase 3 shows an extreme of degradation and devices containing IDTBR would have degraded long before this stage of molecular degradation.

Similar Raman and PL spectra from *in situ* degradation studies of IDFBR are shown in Figure S9. Interestingly it also shows a similar 3-phase degradation process (Figure 2b), although the first phase is dramatically accelerated, and phases 1 and 2 overlap. Phase 1 again consists of a quenching of the main $S_1 \rightarrow S_0$ emission, and a rotation about the IDF-BT dihedral as seen by the relative intensity of the phenyl and BT peaks. The background PL begins to increase with the first few measurements. By following the whole PL spectrum as a function of degradation time, there is also a slight blue-shift of the main PL peak, which could be caused by the increasing band gap expected for more twisted molecules. However, in the 8 hour solar degraded sample, there is a distinct high energy emission at

550 nm (Figure S7), even after the IDFBR absorption is quenched, suggesting that this is a new emissive species formed upon degradation. This is confirmed by PL decay measurements of the two samples, which show different PL decay lifetimes for the fresh and degraded samples with the fresh sample dominated by a mono-exponential process whilst the degraded decay requires multiple exponential components to fit (**Figure S10**). Similarly to IDTBR this high energy PL can be assigned to a degradation (fragmentation) induced product, with a reduced conjugation length. Phase 3 is more distinct for IDFBR, being defined at the peak of high energy PL, after which this PL begins to decrease.

The origin of the conformational change observed is unlikely to be purely photo-induced, as simulated excited states of IDTBR and IDFBR in gas phase show planar geometries (**Figure S11**). However, non-covalent interactions between environmental and conjugated molecules have previously been shown to affect the potential-energy surface (PES) of conjugated polymers.[38] A disruption of the smooth PES allows for many more possible conformations to be adopted. We therefore propose that the conformational change observed here for IDTBR and IDFBR is caused by a similar interaction with environmental species, most likely oxygen. This change in dielectric surroundings then allows for new minima energy structures to be adopted. We show that light is required for this conformational change to occur, and therefore suggest that this non-covalent interaction is between excited or charged species of the conjugated or environmental molecules, which are formed upon photo-excitation. Nikolka *et al* show that for the polymer IDTBT, a more twisted backbone conformation is possible in the presence of these environmental species.[38] This allowed increase in the IDT-BT dihedral angle is analogous to the conformational change observed here for IDTBR. This may indicate that this is a common phenomenon for conjugated systems containing BT units. This is supported by our initial photo-degradation studies on IDTBT, which indicate that a similar conformational change, i.e. IDT-BT torsion, may occur upon degradation of the polymer (**Figure S12**). Based on microsecond transient absorption measurements, we also propose that once the molecular conformation change occurs, allowing interactions with oxygen, the dominant mechanism of degradation of these NFAs is triplet mediated formation of reactive singlet oxygen (see **Figure S13** for details).

Interestingly if we degrade IDTBR in an inert N_2 environment it is found to be stable towards this degradation mechanism (**Figure S14**), signifying the importance of oxygen in the conformational change initiated degradation process. It should also be noted that this degradation mechanism also occurs in EH-IDTBR, an isomer of O-IDTBR with branched ethyl-hexyl side chains, as shown in Figure S12. Unlike IDTBR, IDFBR degrades quickly under illumination in an inert atmosphere, showing similar Raman changes to those observed in air (**Figure S15**). The spectral changes observed are thus due to fragmentation signatures, as indicated previously in the mass spectra of the degraded samples in air. As IDFBR is already twisted it is already prone to the second step of rapid photo-degradation.

The results obtained so far helps us to understand the improvement of stability of IDTBR upon increasing molecular planarity and crystallinity. The conformational change and diffusion of oxygen will both be restricted by a more closely packed molecular lattice, explaining why the annealed IDTBR films show an improvement in stability. This improvement of stability with increasing crystallinity has also been observed for the small molecule donor BTR, which similarly involves a conformational change upon degradation in nitrogen.[31] Therefore our observation reinforces the importance of crystallinity of NFAs for OPV stability.

2.4 Blends with P3HT

Having investigated the degradation mechanism of IDTBR and IDFBR in neat films we now turn our attention to their morphology and stability when blended with P3HT.

Absorption spectra of the as-cast and annealed blends are shown in **Figure 4a**, with annealed neat P3HT absorption shown for comparison. Neat P3HT itself shows no noticeable change in absorption upon annealing at 130°C for 10 minutes (**Figure S16**). However, in the P3HT:IDTBR blend there is a clear increase in IDTBR crystallinity upon annealing, as shown by a 47 nm red-shift of the IDTBR peak at 682 nm, analogous to the shift observed in the neat film. By deconvoluting the as-cast P3HT:IDTBR blend spectra we observe a decrease in the relative intensity of the shoulder at 600 nm (assigned to P3HT aggregation[27]) compared to the neat P3HT films, which indicates P3HT aggregation is being somewhat inhibited by blending with IDTBR. Upon annealing the P3HT:IDTBR blend, there is an increase in the relative intensity of this shoulder showing an increase in P3HT aggregation. This

is more easily discerned in the P3HT:IDFBR blend, in which a shoulder at 600 nm shows a significant increase in relative intensity upon annealing, again signifying an increase in P3HT aggregation. IDFBR absorption shows no change upon annealing in the blend analogous to the neat IDFBR films.

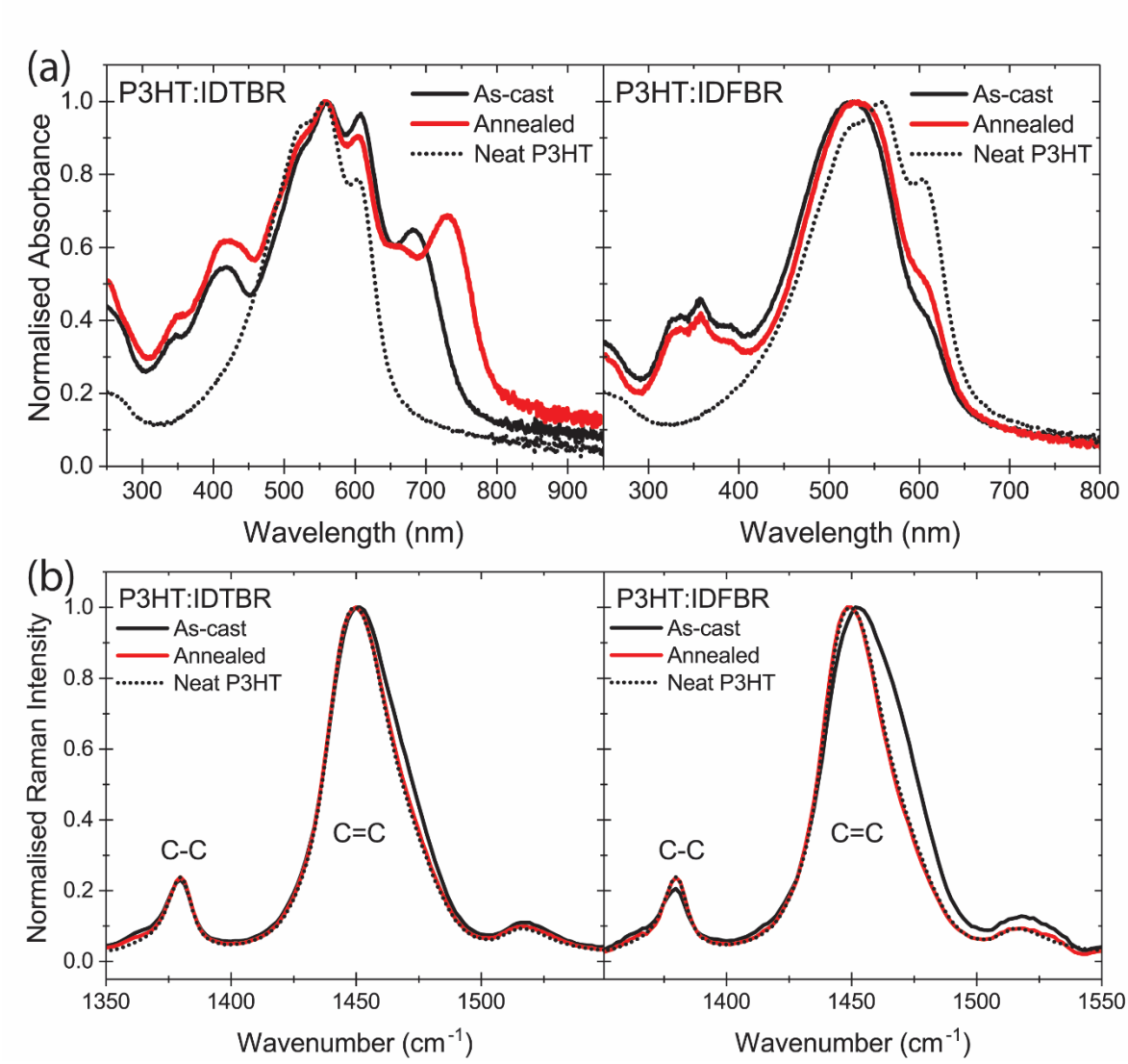

Figure 4. (a) Normalised UV/vis absorption spectra of as-cast and annealed (130°C, 10 minutes) P3HT:IDTBR (left) and P3HT:IDFBR (right) 1:1 blend films plotted with neat annealed P3HT absorption for reference. (b) Normalised Raman spectra of P3HT:IDTBR (left) and P3HT:IDFBR (right) as-cast and annealed blend films at 457 nm excitation. The P3HT:IDFBR spectra have been deconvoluted to show only the vibrational modes of P3HT, again neat, annealed P3HT is plotted for comparison.

Figure 4b comprises the normalised Raman spectra of P3HT within the blends. To investigate the P3HT peaks, the P3HT:IDFBR spectra were deconvoluted whilst this was unnecessary for the IDTBR blend due to the relatively small Raman cross section of IDTBR compared to P3HT. Tsoi *et al*

show that as P3HT order (i.e. backbone planarity) is reduced there is a shift of the main C=C Raman peak (*ca.* 1450 cm^{-1}) to higher frequencies, and the relative intensity of the C-C peak (*ca.* 1380 cm^{-1}) decreases as the effective conjugation length and therefore π-electron delocalisation, is reduced.[27] A very small increase in the FWHM (1 cm^{-1}) of the P3HT C=C mode is observed in the as-cast P3HT:IDTBR blend compared to neat as-cast P3HT, suggesting there is only a very minor disruption of P3HT molecular order by blending with planar IDTBR. In contrast the P3HT C=C peak in the as-cast P3HT:IDFBR blend shows much larger broadening (5 cm^{-1}) and a 4 cm^{-1} peak shift to higher frequencies, indicating a significant disruption of P3HT order, i.e. twisted IDFBR is more miscible with P3HT. Upon annealing, P3HT order in both the P3HT and P3HT:IDTBR (Figure 4b) films increases slightly, shown by a reduction in the main P3HT peak FWHM of 3 cm^{-1}. Annealing the P3HT:IDFBR blend results in a shift of the C=C peak to lower frequencies and a significant narrowing of the FWHM signifying a restoration of P3HT order upon annealing (Figure 4b). These findings are supported by the PL spectra of the as-cast and annealed polymer, and blend films which are shown in **Figure S17**. The P3HT and IDTBR components of PL in the blend follow their neat film PL changes upon annealing indicating a well separated morphology. In the P3HT:IDFBR blend however, there is substantial increase in intensity of the overlapping emission feature which is indicative of phase separation.[26] AFM images (Figure S17) of both blends show an increase in roughness upon annealing confirming increased P3HT and IDTBR crystallinity.

Morphological studies carried out previously using differential scanning calorimetry and X-ray techniques also show that IDFBR is more miscible with P3HT than IDTBR.[20,21] Our observations confirm the idea that the twisted IDFBR molecules are miscible with P3HT, leading to a disruption of polymer molecular order. Upon annealing there seems to be a certain degree of phase separation between IDFBR and P3HT resulting in, to some degree, the recovery of P3HT molecular order and aggregation. The planar IDTBR molecules, on the other hand, are less miscible with P3HT so no significant disruption of P3HT molecular order in the blend is observed in the absorption, Raman or PL spectra. P3HT and IDTBR retain their neat film properties in the as-cast blend films and exhibit the same annealing effects indicating that P3HT and IDTBR form a well phase-separated morphology in

blend, even before thermal treatment. This highlights the importance of acceptor molecular structure on blend morphology.

2.5 Blend Stability

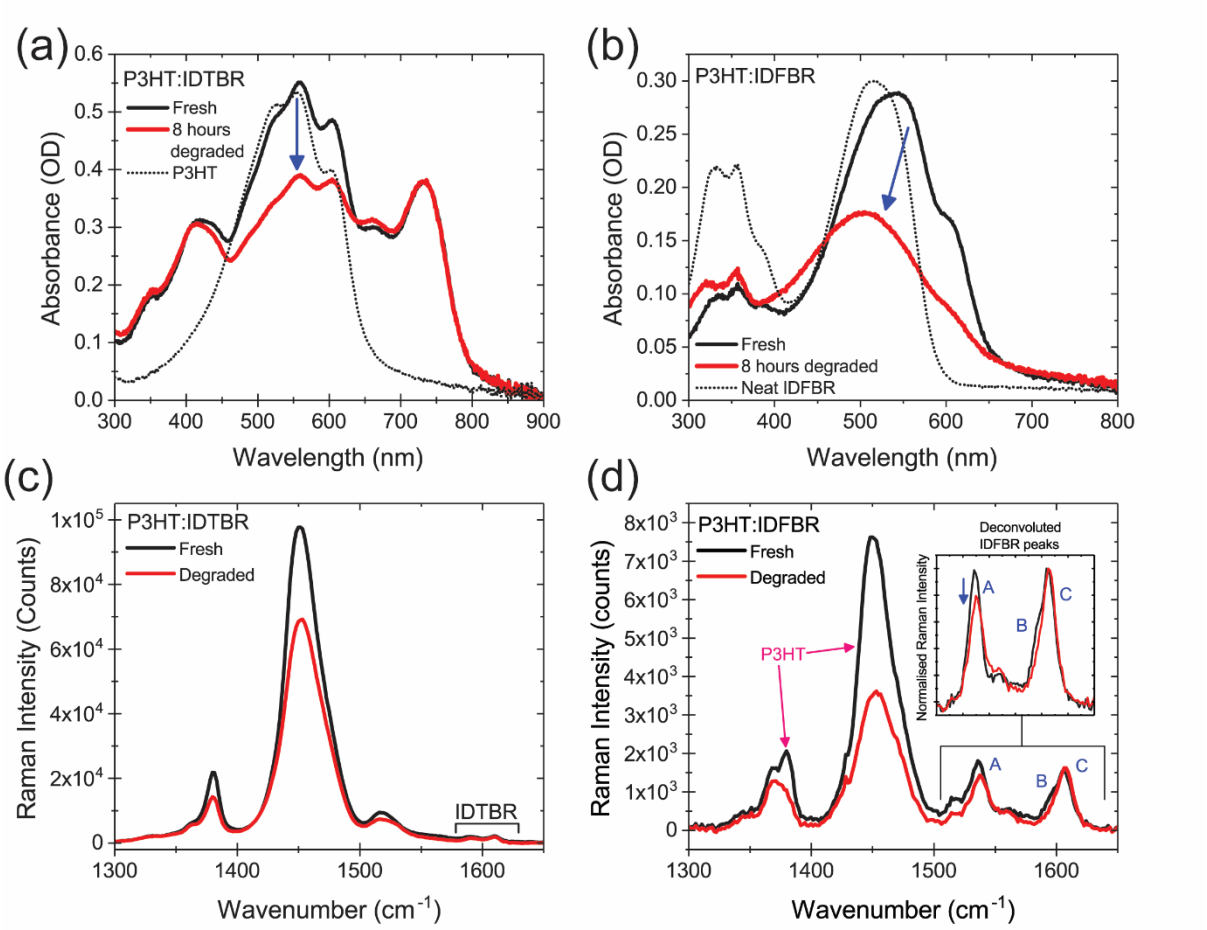

Figure 5. (a+b) UV/vis absorption spectra of fresh and degraded (solar illumination in air) P3HT:IDTBR (a) and P3HT:IDFBR (b) blend films with fresh P3HT (a) and fresh IDFBR (b) absorption spectra for reference. (c) Baseline corrected Raman spectra of P3HT:IDTBR at 457 nm excitation. (d) Baseline corrected Raman spectra of P3HT:IDFBR at 457 nm excitation the main P3HT modes are labelled, whilst the inset shows the normalised and deconvoluted IDFBR Raman peaks within the blend, labelled (A), (B) and (C).

To investigate the photostability of the blends, annealed blend and neat P3HT films were degraded under 1 sun illumination in air, in the same way as the neat NFA films. **Figure 5a** shows the absorption spectra of P3HT:IDTBR blend films before and after degradation. There is a 27% intensity bleaching of the P3HT absorption centred at *ca.* 550 nm, analogous to the 25% bleaching of intensity upon equivalent degradation of neat P3HT (**Figure S18**). However, the IDTBR absorption is not

bleached upon degradation in the blend after 8 hours, comparable to the annealed IDTBR neat film (Figure S8) Indicating that the well separated morphology of P3HT and IDTBR does not lead to any obvious stabilising or destabilising effects on this timescale of degradation.

Figure 5b shows the absorption spectra of P3HT:IDFBR before and after solar illumination in air. There is a strong bleaching and blue-shift of the main overlapping absorption band, whilst the IDFBR absorption peak between 300-400 nm is not bleached. It is important to notice that after 8 hours of degradation of neat IDFBR there was a complete bleaching of both absorption bands of IDFBR (Figure 2a), whereas in the blend there is still clear high energy IDFBR absorption, indicating that IDFBR is stabilised in the blend. In contrast, the intensity of the P3HT aggregate shoulder at 608 nm is significantly reduced by 50% in the blend whereas in the neat film this is bleached by only 30%, suggesting P3HT becomes less stable, with its degradation accelerated when blended with IDFBR. P3HT absorption quenching of this nature has been observed and is attributed to a reduction in π-conjugation length caused by radical oxygen driven oxidation of the thiophene moieties.[39–41] Akin to the absorption changes, the Raman spectra of the fresh and degraded samples in Figure 5c and 5d, show a selective bleaching of the P3HT modes (*ca.* 1380, 1450 and 1515 cm^{-1}). The intensity of the main P3HT peak is quenched significantly more when blended with IDFBR (>50%) compared to when blended with IDTBR (~30%), reinforcing the claim that the twisted acceptor reduces the polymer stability.

Now, we look at the changes in the acceptors. The deconvoluted Raman spectra of IDFBR in the blend is shown in the inset of Figure 5d. After 8 hours of degradation there is a decrease in the relative intensity of the BT peak (A) at 1536 cm^{-1}, and a narrowing and slight shift of peak C to higher frequencies, indicating the same degradation process as observed in the neat film. Although these changes are much smaller than in the neat IDFBR film (Figure 2d), the result confirms the same conformational change occurring during photodegradation in the blend and much less stable nature of the twisted IDFBR acceptor.

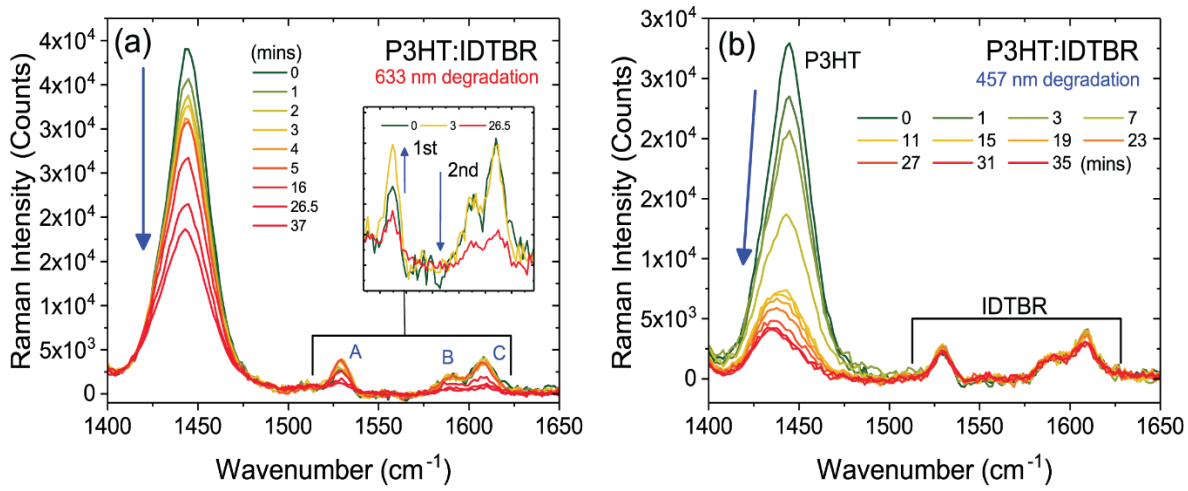

Figure 6. Baseline corrected in situ Raman spectra at increasing laser illumination times in air, at time 0 the films have already been illuminated for 8 hours in a solar simulator in air, the probe excitation for both measurements is 633 nm, the degradation lasers were 633 nm (a) and 457 nm (b).

The observations so far allow us to conclude that IDFBR is stabilised in the blend, to investigate if this is also true for IDTBR, accelerated *in situ* degradation studies on the P3HT:IDTBR blend were carried out. **Figure 6a** shows the Raman spectra obtained during *in situ* degradation of the blend using 633 nm illumination. At this wavelength both P3HT and IDTBR have significant absorption. There is an instant bleaching of the P3HT C=C peak, with a slight broadening to lower frequencies (**Figure S19**). The intensity of peak C of IDTBR (1608 cm^{-1}) initially stays constant whilst the relative intensity of peak A (1530 cm^{-1}) increases in intensity, analogous to the initial Raman peak changes observed during *in situ* neat film degradation and attributed to a molecular conformational twisting of the IDTBR backbone (Figure 3a,b). The inset shows that this initial molecular conformational change, is followed by a quenching of all IDTBR peaks, signifying that the three phase degradation process observed in the neat films is also occurring in the blend.

It is important to consider the impact of such conformational changes of the NFA molecules on the photostability of photovoltaic blends. Interfacial energetics, determined by donor and acceptor energy levels (in particular the LUMO level of the acceptor), are critical for photophysical processes of photovoltaic devices such as charge generation. The conformational changes of NFAs towards more twisted structures upon illumination in air would shift their LUMO energy levels to shallower energies

(Figure S4), reducing the interfacial energy offset between donor and acceptor affecting photophyscial processes and their stability. In ongoing work we demonstrate that the donor polymer stability in the blend is dependent on the LUMO level of the acceptors, which explains why P3HT is less stable when blended with the acceptor with the shallower LUMO, here IDFBR.

Accelerated degradation studies using the 457 nm excitation as a degradation source were also carried out (Figure 6b), for comparison with the neat film *in situ* degradation outlined in Figure 3. As with 633 nm degradation, there is a significant bleaching of the P3HT C=C mode. Surprisingly, after *ca.*30 minutes of 457 nm illumination there are negligible changes in the IDTBR Raman peaks, in contrast to the neat films which show clear conformational changes within 30 seconds of 457 nm illumination. P3HT absorbs strongly at 457 nm whilst IDTBR has only a small absorption so one would expect a disproportionate degradation of P3HT, however, it is shown that at this wavelength rapid degradation of IDTBR is also possible in the neat film, we therefore suggest that IDTBR is more stable in the blend compared to the neat film. Our results indicate that both NFAs are stabilised in the blend, and we assign this stabilisation to excited state quenching via charge generation with the polymer, reducing the excited state degradation observed in the neat films.

To investigate P3HT photo-degradation further HOMO energy levels were measured using APS. **Figure 7a** shows the extracted HOMO energy levels for fresh and degraded films (APS spectra can be found in **Figure S20**). There is a deepening of the P3HT HOMO level from 4.50 ± 0.05 to 4.70 ± 0.05 eV upon blending with the NFAs. This may be due to the NFAs disrupting P3HT crystallinity as observed by the reduced aggregate shoulder in the deconvoluted absorption spectra, and similar to previous reports of P3HT energy levels as a function of crystallisation.[42] The measured HOMO energy levels of the as-cast films of both IDTBR and IDFBR are *ca.* 5.60 eV. Upon degradation there is a further deepening of the P3HT HOMO level and additionally a reduction in photoemission yield. Deepening of the HOMO level by 0.65 eV, 0.50 eV, and 0.85 eV is measured for P3HT, P3HT:IDTBR, and P3HT:IDFBR films respectively. The most dramatic change is observed for the P3HT:IDFBR blend, again indicating that P3HT degrades faster in the presence of IDFBR. By blending P3HT with IDTBR, the stability of P3HT is slightly improved relative to the neat film. To see if these changes are

caused by photo-oxidation, as suggested above, the HOMO energy level of P3HT and some potential oxidation products[39,40] were simulated. Both oxidised species show a deeper HOMO level than P3HT (Figure 7b), highlighting the electron withdrawing effect of the electronegative oxygen atom on electron density. They also show smaller optical band gaps than P3HT (**Figure S21**).

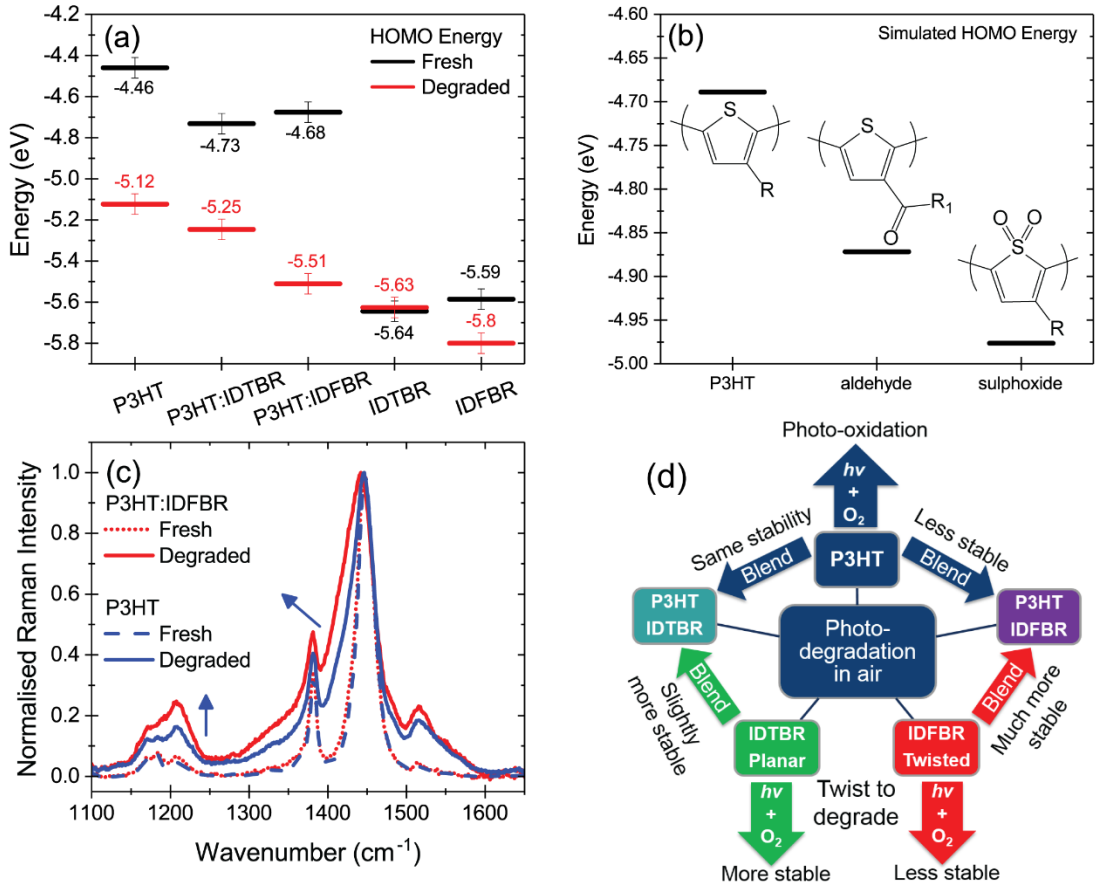

Figure 7. (a) HOMO energy levels obtained using air photoemission spectroscopy (APS) of fresh and degraded films on ITO. (b) simulated HOMO levels (DFT, B3LYP, 6-31G(d,p)) of P3HT pentamers with different potential oxidation products on the central monomer as shown in the inset chemical structures. (c) Normalised Raman spectra of neat P3HT and P3HT:IDFBR at 785 nm excitation. (d) Summary of stabilisation and destabilisation processes in the blends.

The nature of photo-degradation of P3HT was further investigated by resonant Raman spectroscopy using 785 nm excitation which will be resonant with the oxidised species with a smaller optical band gap (Figure 7c). After 8 hours of degradation of the neat and blend films, the main P3HT C=C peak broadens to lower frequencies and there is an increase in relative intensity of the C-C peak at *ca.*1200 cm^{-1}. In the P3HT:IDFBR blend the broadening of the C=C peak and growth of the peak at 1200 cm^{-1}

occurs to a much greater extent, indicating faster degradation of P3HT in the IDFBR blend, confirming our claim that P3HT becomes much less stable when blended with twisted IDFBR. The Raman simulations of the P3HT pentamer containing a sulfoxide unit show similarities to those of the experimentally degraded P3HT (Figure S21), thus providing a possible origin to these observations, these spectral changes have been previously observed upon P3HT degradation in air.[43,44] Note that the Raman features and deeper HOMO appearing in photo-oxidised samples also have a close resemblance with polaronic species formed upon chemical doping of P3HT.[45–47] Figure 7d summarises the stabilisation and destabilisation effects of IDTBR, IDFBR, and P3HT observed between their neat and blend films.

3. Conclusions

In this work we have investigated the effect of molecular structure on the photostability of two non-fullerene acceptors, IDTBR and IDFBR. We have found that under illumination in air these molecules undergo a three-phase degradation process. Initially a photo-induced conformational change occurs, driven by non-covalent interactions with environmental molecules. This allows for a second step of degradation, either photo-oxidation or fragmentation, disrupting the molecular chromophore. This is then followed by the third phase in which the initial chromophores of the molecules are completely bleached. These findings suggest planarity of the conjugated backbone and crystallinity of these small molecule acceptors is beneficial to neat film photostability in both ambient and inert environments. Furthermore, the molecular conformation is found to be important for understanding the miscibility of IDTBR and IDFBR with the semi-crystalline donor polymer P3HT and the photostability of their blends. The amorphous, non-planar IDFBR is more miscible than planar IDTBR with P3HT. When blended, much faster and significant photodegradation of P3HT is observed in P3HT:IDFBR blend compared to P3HT:IDTBR blend. The same three phase degradation process of NFAs is also found in the blends although both show their degradation is slowed down. These results highlight the important role of NFA's molecular structure on photostability of photovoltaic blends.

Based on our observations, we propose molecular design considerations for A-D-A non-fullerene acceptors: firstly, a planar structure of the conjugated backbone is important for stability and

not just for optimising morphology for efficiency; secondly, we speculate that if this planarity was frozen, by the use of fused-systems, or by intramolecular interactions such as sulphur-fluorine interactions[48], it would be possible to inhibit the degradation mechanism observed. We have also introduced some results from molecules containing BT groups which may show similar degradation pathways. We therefore raise the question as to whether there is an intrinsic stability problem when using BT units within conjugated molecules, although further studies are required.

4. Experimental Methods

4.1 Sample preparation

The syntheses of IDTBR and IDFBR have previously been reported.[21] Two batches of regioregular P3HT were used within the blends although both are of a similar M_W and regioregularity (M_W = 51 kDa, ≥96% regioregularity and, M_W = 36 kDa, >99% regioregularity). It has recently been shown that P3HT:IDTBR devices have a P3HT M_W dependent performance due to the sensitivity of morphology to molecular weight.[25] From our measurements we observe very slight differences in morphology depending on sample batch studied but without any major influence on the conclusions presented in this work. Neat NFA solutions were prepared at a concentration of 12 mg ml^{-1} in chloroform, whilst neat P3HT and 1:1 P3HT:NFAs blends were dissolved in chlorobenzene at 10 and 20 mg ml^{-1} respectively. All solutions were stirred overnight at 60°C before thin films were spin coated onto clean glass, ITO or fused quartz substrates to give films with a thickness of 50-100 nm measured with a Dektak profilometer. Films were annealed within a N_2 atmosphere at 130°C for 10 minutes. Degradation of the samples was carried out using a Solaronix solar simulator (Class AAA), at 1 sun illumination (AM1.5) in air with a temperature maintained at ~25°C.

4.2 Spectroscopic measurements

A Shimadzu UV-2550 UV-visible spectrophotometer was used to measure steady state transmittance of substrates and samples. Absorbance was then calculated using the following equation to remove substrate contributions: $Abs = log(T_{Substrate}/T_{Sample})$, with reflection and scattering effects being ignored.

A Renishaw in Via Raman microscope with a 50x objective in a backscattering configuration was used to collect both photoluminescence (PL) and Raman spectra. All measurements, unless otherwise stated, were conducted in a nitrogen-purged Linkam sample chamber. All measurements were taken with a defocussed laser spot with a radius of ~10 μm. PL spectra were recorded using 514 nm laser excitation, with no correction being applied for instrument response. Raman spectra were collected at various wavelengths using an argon ion laser (457, 488 514 nm), a HeNe laser (633 nm) and a diode laser (785 nm). Acquisition times and laser powers for both PL and Raman measurements were optimised to give the best spectra, but were kept consistent between samples that are compared in the results and discussion. Spectrometer calibration was conducted using a silicon reference sample and background PL was subtracted using a polynomial fit.

In situ photo-degradation studies were carried out in both air and nitrogen using the Raman laser excitation source to both degrade the sample and collect Raman or PL spectra simultaneously. Two wavelengths are used for these studies, 633 nm and 457 nm. The 457 nm laser has an estimated power density at the sample of ~2 x 10^6 W m^{-2}, three orders of magnitude larger than 1 sun illumination at 1 x 10^3 W m^{-2}, allowing for accelerated degradation studies. The approximate power density of the 633 nm laser used for *in* situ degradation is ~8 x 10^6 W m^{-2}, ~4x that of the 457 nm laser used. Where two different wavelengths have been used for degradation and data collection, Raman or PL spectra were taken in nitrogen, whilst degradation was conducted in air. The 633 nm excitation is highly resonant with the lower energy absorption of IDTBR enhancing the PL and Raman intensity of the IDTBR vibrational modes. Due to this the *in situ* experiments of the P3HT:IDTBR blend were conducted on the 8 hour solar simulator degraded samples which show a quenching of this PL, allowing for Raman spectra collection.

4.3 Energetics and Morphology

Ambient photoemission measurements were taken using an APS04 Air Photoemission system (APS04, by KP Technology) using a 2 mm gold tip under atmospheric conditions. All samples were measured on ITO substrates to ensure proper grounding of the organic thin films. Measurements were taken at multiple positions on the films to ensure reproducibility. The APS data was processed using

the protocol described by Baike et al.[49] This involves taking the cube root of the measured photoemission, fitting the resultant linear region and extrapolating to zero photoemission to find the HOMO level of the semiconductor. Atomic force microscopy (AFM) measurements were taken using a Park NX10 AFM system and SmartScan™ software with Park silicon PPP-NCHR tips.

4.4 Computational Methods

Density functional theory (DFT) calculations were conducted using GAUSSAIN09 software on the Imperial College High-Performance Computing service.[50] All simulations have been carried out as single molecules in the gas phase at the B3LYP level of theory with the basis set 6-31G(d,p).[51–54] Alkyl side chains were simplified to methyl groups to reduce computational time and polymers were modelled as pentamers with methyl capping units. Structures were optimised to a local minimum energy conformation with frozen dihedral angles being used to simulate molecular conformational changes. Frequency calculations were carried out to simulate the Raman spectra, an empirical scaling factor of 0.97 was used for the frequency of vibration.[55] Visualisation of the simulated vibrational modes using GaussView 6.0.16 software was used to aid Raman peak assignment alongside consultation with the literature.[32,33,56,57]

Supporting Information

Supporting Information is available from the Wiley Online Library or from the author.

Acknowledgments

The authors acknowledge the UK EPSRC for the Plastic Electronics Centre for Doctoral Training (EP/G037515/1) funding and CSEM Brasil for studentship. E. M. S, W. C. T. and Z. L. thank the National Research Network in Advanced Engineering Materials (grant number NRN093), the Welsh Assembly Government funded Ser Cymru Solar Project and UK EPSRC (EP/M025020/1). Thanks to John de Mello and James Bannock of Imperial College London for providing some of the P3HT used, and to the Imperial College High Performance Computing Service for DFT calculations.

Received:
Revised:
Published online:

References

[1] D. Deng, Y. Zhang, J. Zhang, Z. Wang, L. Zhu, J. Fang, B. Xia, Z. Wang, K. Lu, W. Ma, Z. Wei, *Nat. Commun.* **2016**, *7*, 13740.

[2] J. Zhao, Y. Li, G. Yang, K. Jiang, H. Lin, H. Ade, W. Ma, H. Yan, *Nat. Energy* **2016**, *1*, 15027.

[3] C. H. Peters, I. T. Sachs-Quintana, J. P. Kastrop, S. Beaupré, M. Leclerc, M. D. McGehee, *Adv. Energy Mater.* **2011**, *1*, 491.

[4] C. B. Nielsen, S. Holliday, H.-Y. Chen, S. J. Cryer, I. McCulloch, *Acc. Chem. Res.* **2015**, *48*, 2803.

[5] T. Heumueller, W. R. Mateker, A. Distler, U. F. Fritze, R. Cheacharoen, W. H. Nguyen, M. Biele, M. Salvador, M. von Delius, H.-J. Egelhaaf, M. D. McGehee, C. J. Brabec, *Energy Environ. Sci.* **2015**, *9*, 247.

[6] A. Distler, T. Sauermann, H. J. Egelhaaf, S. Rodman, D. Waller, K. S. Cheon, M. Lee, D. M. Guldi, *Adv. Energy Mater.* **2014**, *4*, 1300693.

[7] N. Deb, R. R. Dasari, K. Moudgil, J. L. Hernandez, S. R. Marder, Y. Sun, A. Karim, D. G. Bucknall, *J. Mater. Chem. A* **2015**, *3*, 21856.

[8] B. C. Schroeder, Z. Li, M. A. Brady, G. C. Faria, R. S. Ashraf, C. J. Takacs, J. S. Cowart, D. T. Duong, K. H. Chiu, C. H. Tan, J. T. Cabral, A. Salleo, M. L. Chabinyc, J. R. Durrant, I. McCulloch, *Angew. Chemie - Int. Ed.* **2014**, *53*, 12870.

[9] Z. Li, H. C. Wong, Z. Huang, H. Zhong, C. H. Tan, W. C. Tsoi, J. S. Kim, J. R.

Durrant, J. T. Cabral, *Nat. Commun.* **2013**, *4:2227*, DOI 10.1038/ncomms3227.

[10] H. K. H. Lee, A. M. Telford, J. A. Röhr, M. F. Wyatt, B. Rice, J. Wu, A. De Castro Maciel, S. M. Tuladhar, E. Speller, J. McGettrick, J. R. Searle, S. Pont, T. Watson, T. Kirchartz, J. R. Durrant, W. C. Tsoi, J. Nelson, Z. Li, *Energy Environ. Sci.* **2018**, *11*, 417.

[11] E. M. Speller, J. D. McGettrick, B. Rice, A. M. Telford, H. K. H. Lee, C. H. Tan, C. S. De Castro, M. L. Davies, T. M. Watson, J. Nelson, J. R. Durrant, Z. Li, W. C. Tsoi, *ACS Appl. Mater. Interfaces* **2017**, *9*, 22739.

[12] W. Zhao, S. Li, H. Yao, S. Zhang, Y. Zhang, B. Yang, J. Hou, *J. Am. Chem. Soc.* **2017**, *139*, 7148.

[13] Z. Fei, F. D. Eisner, X. Jiao, M. Azzouzi, J. A. Röhr, Y. Han, M. Shahid, A. S. R. Chesman, C. D. Easton, McNeill Christopher R., Anthopoulos Thomas D., J. Nelson, M. Heeney, *Adv. Mater.* **2018**, *30*, 1705209.

[14] N. Gasparini, M. Salvador, S. Strohm, T. Heumueller, I. Levchuk, A. Wadsworth, J. H. Bannock, J. C. de Mello, H.-J. Egelhaaf, D. Baran, I. McCulloch, C. J. Brabec, *Adv. Energy Mater.* **2017**, 1700770.

[15] H. Cha, J. Wu, A. Wadsworth, J. Nagitta, S. Limbu, S. Pont, Z. Li, J. Searle, M. F. Wyatt, D. Baran, J. S. Kim, I. Mcculloch, J. R. Durrant, *Adv. Mater.* **2017**, 1701156.

[16] A. Wadsworth, R. S. Ashraf, M. Abdelsamie, S. Pont, M. Little, M. Moser, Z. Hamid, M. Neophytou, W. Zhang, A. Amassian, J. R. Durrant, D. Baran, I. McCulloch, *ACS Energy Lett.* **2017**, *2*, 1494.

[17] Y. Yang, Z. G. Zhang, H. Bin, S. Chen, L. Gao, L. Xue, C. Yang, Y. Li, *J. Am. Chem. Soc.* **2016**, *138*, 15011.

[18] Y. J. Hwang, H. Li, B. A. E. Courtright, S. Subramaniyan, S. A. Jenekhe, *Adv. Mater.* **2016**, *28*, 124.

[19] S. Holliday, R. S. Ashraf, C. B. Nielsen, M. Kirkus, J. A. Röhr, C. H. Tan, E. Collado-Fregoso, A. C. Knall, J. R. Durrant, J. Nelson, I. McCulloch, *J. Am. Chem. Soc.* **2015**, *137*, 898.

[20] S. Holliday, R. S. Ashraf, A. Wadsworth, D. Baran, S. A. Yousaf, C. B. Nielsen, C.-H. Tan, S. D. Dimitrov, Z. Shang, N. Gasparini, M. Alamoudi, F. Laquai, C. J. Brabec, A. Salleo, J. R. Durrant, I. McCulloch, *Nat. Commun.* **2016**, *7:11585*, DOI 10.1038/ncomms11585.

[21] D. Baran, R. A. S. Ashraf, D. A. Hanifi, M. Abdelsamie, N. Gasparini, J. A. Röhr, S. Holliday, A. Wadsworth, S. Lockett, M. Neophytou, C. J. M. Emmott, J. Nelson, C. J. Brabec, A. Amassian, T. Kirchartz, J. R. Durrant, I. Mcculloch, D. Baran, R. A. S. Ashraf, S. Holliday, A. Wadsworth, S. Lockett, P. J. R. Durrant, *Nat. Mater.* **2016**, *16*, 363.

[22] W. Zhao, D. Qian, S. Zhang, S. Li, O. Inganäs, F. Gao, J. Hou, *Adv. Mater.* **2016**, *28*, 4734.

[23] Z. Li, K. Jiang, G. Yang, J. Y. L. Lai, T. Ma, J. Zhao, W. Ma, H. Yan, *Nat. Commun.* **2016**, *7:13094*, DOI 10.1038/ncomms13094.

[24] F. Zhao, S. Dai, Y. Wu, Q. Zhang, J. Wang, L. Jiang, Q. Ling, Z. Wei, W. Ma, W. You, C. Wang, X. Zhan, *Adv. Mater.* **2017**, *29*, 1700144.

[25] A. Wadsworth, Z. Hamid, M. Bidwell, R. S. Ashraf, J. Khan, C. Cendra, J. Yan, E. R. Soltani, A. A. Y. Guilbert, A. Salleo, J. Nelson, F. Laquai, I. Mcculloch, *Adv. Energy Mater.* **2018**, 1801001.

[26] J. Razzell-Hollis, S. Limbu, J. S. Kim, *J. Phys. Chem. C* **2016**, *120*, 10806.

[27] W. C. Tsoi, D. T. James, J. S. Kim, P. G. Nicholson, C. E. Murphy, D. D. C. Bradley, J. Nelson, J. S. Kim, *J. Am. Chem. Soc.* **2011**, *133*, 9834.

[28] S. Wood, J. R. Hollis, J.-S. S. Kim, *J. Phys. D. Appl. Phys.* **2017**, *50*, 073001.

[29] J. Razzell-Hollis, J. Wade, W. C. Tsoi, Y. Soon, J. Durrant, J.-S. Kim, *J. Mater. Chem. A Mater. Energy Sustain.* **2014**, *2*, 20189.

[30] S. Wood, J. Wade, M. Shahid, E. Collado-Fregoso, D. D. C. Bradley, J. R. Durrant, M. Heeney, J.-S. Kim, *Energy Environ. Sci.* **2015**, *8*, 3222.

[31] M. J. Newman, E. M. Speller, J. Barbé, J. Luke, M. Li, Z. Li, Z. K. Wang, S. M. Jain, J. S. Kim, H. K. H. Lee, W. C. Tsoi, *Sci. Technol. Adv. Mater.* **2018**, *19*, 194.

[32] J. P. Schmidtke, J. S. Kim, J. Gierschner, C. Silva, R. H. Friend, *Phys. Rev. Lett.* **2007**, *99*, 167401.

[33] D. Venkateshvaran, M. Nikolka, A. Sadhanala, V. Lemaur, M. Zelazny, M. Kepa, M. Hurhangee, A. J. Kronemeijer, V. Pecunia, I. Nasrallah, I. Romanov, K. Broch, I. McCulloch, D. Emin, Y. Olivier, J. Cornil, D. Beljonne, H. Sirringhaus, *Nature* **2014**, *515*, 384.

[34] K. G. Jespersen, W. J. D. Beenken, Y. Zaushitsyn, A. Yartsev, M. Andersson, T. Pullerits, V. Sundström, *J. Chem. Phys.* **2004**, *121*, 12613.

[35] M. S. Vezie, S. Few, I. Meager, G. Pieridou, B. Dörling, R. S. Ashraf, A. R. Goñi, H. Bronstein, I. McCulloch, S. C. Hayes, M. Campoy-Quiles, J. Nelson, *Nat. Mater.* **2016**, *15*, 746.

[36] S. Scholz, D. Kondakov, B. Lüssem, K. Leo, *Chem. Rev.* **2015**, *115*, 8449.

[37] W. Song, J. Y. Lee, *Adv. Opt. Mater.* **2017**, *5*, 1600901.

[38] M. Nikolka, I. Nasrallah, B. Rose, M. K. Ravva, K. Broch, A. Sadhanala, D. Harkin, J. Charmet, M. Hurhangee, A. Brown, S. Illig, P. Too, J. Jongman, I. McCulloch, J. L. Bredas, H. Sirringhaus, *Nat. Mater.* **2017**, *16*, 356.

[39] M. Manceau, A. Rivaton, J. L. Gardette, S. Guillerez, N. Lemaître, *Polym. Degrad. Stab.* **2009**, *94*, 898.

[40] M. Manceau, J. Gaume, A. Rivaton, J. L. Gardette, G. Monier, L. Bideux, *Thin Solid Films* **2010**, *518*, 7113.

[41] J. Ficker, H. Von Seggern, H. Rost, W. Fix, W. Clemens, I. McCulloch, *Appl. Phys. Lett.* **2004**, *85*, 1377.

[42] W. C. Tsoi, S. J. Spencer, L. Yang, A. M. Ballantyne, P. G. Nicholson, A. Turnbull, A. G. Shard, C. E. Murphy, D. D. C. Bradley, J. Nelson, J. S. Kim, *Macromolecules* **2011**, *44*, 2944.

[43] G. M. Paternò, V. Robbiano, K. J. Fraser, C. Frost, V. Garciá Sakai, F. Cacialli, V. García Sakai, F. Cacialli, *Sci. Rep.* **2017**, *7*, 41013.

[44] S. Bellani, D. Fazzi, P. Bruno, E. Giussani, E. V. Canesi, G. Lanzani, M. R. Antognazza, *J. Phys. Chem. C* **2014**, *118*, 6291.

[45] E. A. Bazzaoui, G. Lévi, S. Aeiyach, J. Aubard, J. P. Marsault, P. C. Lacaze, *J. Phys. Chem.* **1995**, *99*, 6628.

[46] M. Baibarac, M. Lapkowski, A. Pron, S. Lefrant, I. Baltog, *J. Raman Spectrosc.* **1998**, *29*, 825.

[47] E. Alveroglu, *J. Mol. Struct.* **2015**, *1086*, 86.

[48] S. Wood, J. H. S. Kim, D. H. Hwang, J. H. S. Kim, *Chem. Mater.* **2015**, *27*, 4196.

[49] I. D. Baikie, A. C. Grain, J. Sutherland, J. Law, in *Energy Procedia*, Elsevier, **2014**, pp. 48–56.

[50] M. J. Frisch, G. W. Trucks, H. B. Schlegel, G. E. Scuseria, M. A. Robb, J. . Cheeseman, G. Scalmani, V. Barone, B. Mennucci, G. A. Petersson, H. Nakatsuji, M. Caricato, X. Li, H. P. Hratchian, A. F. Izmaylov, J. Bloino, G. Zheng, J. L. Sonnenberg, M. Hada, M. Ehara, K. Toyota, R. Fukuda, J. Hasegawa, M. Ishida, T. Nakajima, Y. Honda, O. Kitao, H. Nakai, T. Vreven, J. A. Montgomery Jr., J. E. Peralta, F. Ogliaro, M. Bearpark, J. J. Heyd, E. Brothers, K. N. Kudin, V. N. Staroverov, R. Kobayashi, J. Normand, K. Raghavachari, A. Rendell, J. C. Burant, S. S. Iyengar, J. Tomasi, M. Cossi, N. Rega, J. M. Millam, M. Klene, J. E. Knox, J. B. Cross, V. Bakken, C. Adamo, J. Jaramillo, R. Gomperts, R. E. Stratmann, O. Yazyev, A. J. Austin, R. Cammi, C. Pomelli, J. W. Ochterski, R. L. Martin, K. Morokuma, V. G. Zakrzewski, G. A. Voth, P. Salvador, J. J. Dannenberg, S. Dapprich, A. D. Daniels, O. Farkas, J. B. Foresman, J. V. Ortiz, J. Cioslowski, D. J. Fox, **2009**.

[51] A. D. Becke, *J. Chem. Phys.* **1993**, *98*, 5648.

[52] G. A. Petersson, M. A. Al-Laham, *J. Chem. Phys.* **1991**, *94*, 6081.

[53] G. A. Petersson, A. Bennett, T. G. Tensfeldt, M. A. Al-Laham, W. A. Shirley, J. Mantzaris, *J. Chem. Phys.* **1988**, *89*, 2193.

[54] P. J. Stephens, F. J. Devlin, C. F. Chabalowski, M. J. Frisch, *J. Phys. Chem.* **1994**, *98*, 11623.

[55] M. L. Laury, M. J. Carlson, A. K. Wilson, *J. Comput. Chem.* **2012**, *33*, 2380.

[56] S. Wood, J. S. Kim, D. T. James, W. C. Tsoi, C. E. Murphy, J.-S. Kim, *J. Chem. Phys.*

2013, *139*, 064901.

[57] X. Rodriguez-Martinez, M. S. Vezie, X. Shi, I. McCulloch, J. Nelson, A. R. Goñi, M. Campoy-Quiles, *J. Mater. Chem. C* **2017**, *5*, 7270.

TOC

Non-fullerene acceptors (NFAs) provide an exciting prospect for organic solar cells, however their stability still lacks fundamental understating. The promising high efficiency NFAs, IDTBR and IDFBR, show a three-phase degradation mechanism, which involves a strong initial molecular conformational change prior to photo-degradation under light and oxygen stress, indicating the importance role of NFA molecular structure on solar cell stability.

Keyword: Organic Solar Cells

Joel Luke, Emily M. Speller, Andrew Wadsworth, Mark F. Wyatt, Stoichko Dimitrov, Zhe Li, Wing C. Tsoi, Iain McCulloch, Diego Bagnis, James R. Durrant, Ji-Seon Kim*

Twist and Degrade – Impact of Molecular Structure on the Photostability of Non-Fullerene Acceptors and Their Photovoltaic Blends

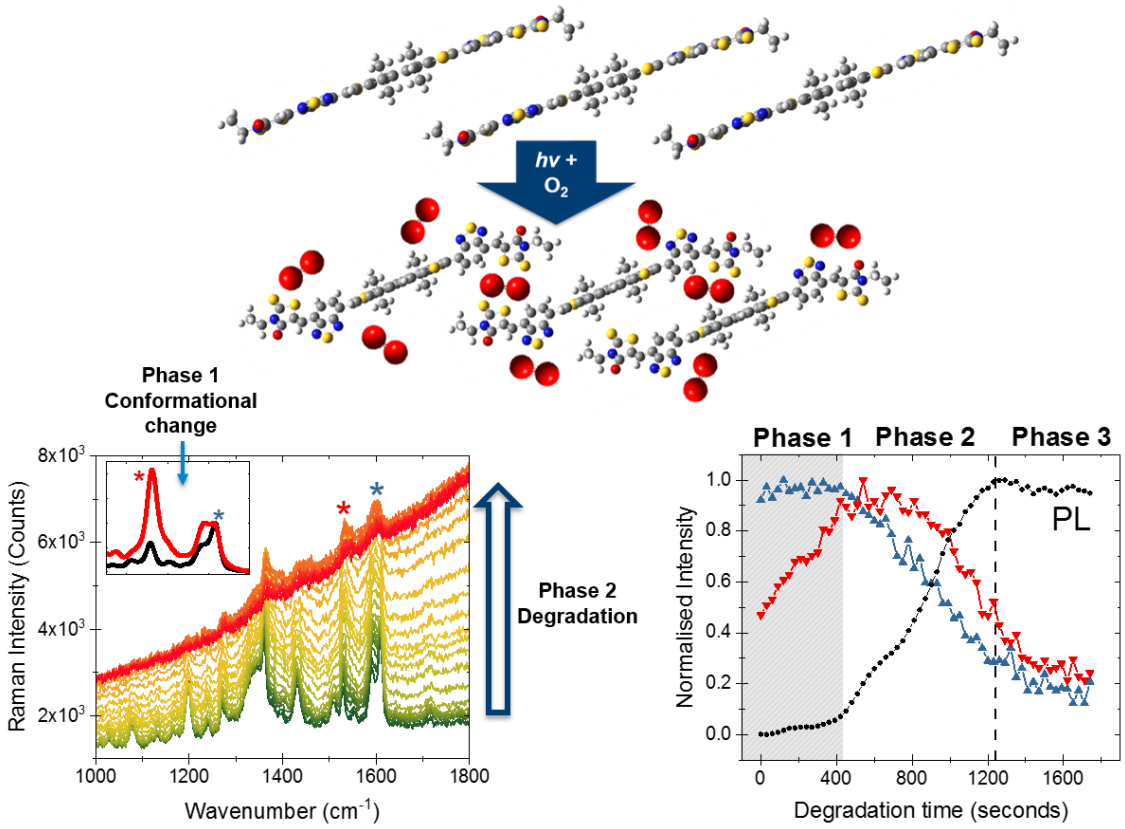

Electronic Supplementary Information

Twist and Degrade – Impact of Molecular Structure on the Photostability of Non-Fullerene Acceptors and Their Photovoltaic Blends

Joel Luke[a], *Emily M. Speller*[b], *Andrew Wadsworth*[c], *Mark F. Wyatt*[d], *Stoichko Dimitrov*[b], *Zhe Li*[e], *Wing C. Tsoi*[b], *Iain McCulloch*[c,f], *Diego Bagnis*[g], *James R. Durrant*[b, c], *Ji-Seon Kim**[a]

(a) Department of Physics and Centre for Plastic Electronics, Imperial College London, London, SW7 2AZ, UK. E-mail: ji-seon.kim@imperial.ac.uk

(b) SPECIFIC IKC, College of Engineering, Swansea University, Bay Campus, Fabian Way, Swansea, Wales, SA1 8EN, UK

(c) Department of Chemistry and Centre for Plastic Electronics, Imperial College London, London SW7 2AY, UK

(d) EPSRC UK National Mass Spectrometry Facility (NMSF), Swansea University Medical School, Singleton Park, Swansea SA2 8PP, UK

(e) School of Engineering, Cardiff University, CF24 3AA, UK

(f) KSC King Abdullah University of Science and Technology, Thuwal, 23955-6900, Saudi Arabia

(g) Centro de Inovações, CSEM BRASIL, Av. José Cândido da Silveira, 2000 - Horto Florestal, Belo Horizonte - MG, 31035-536

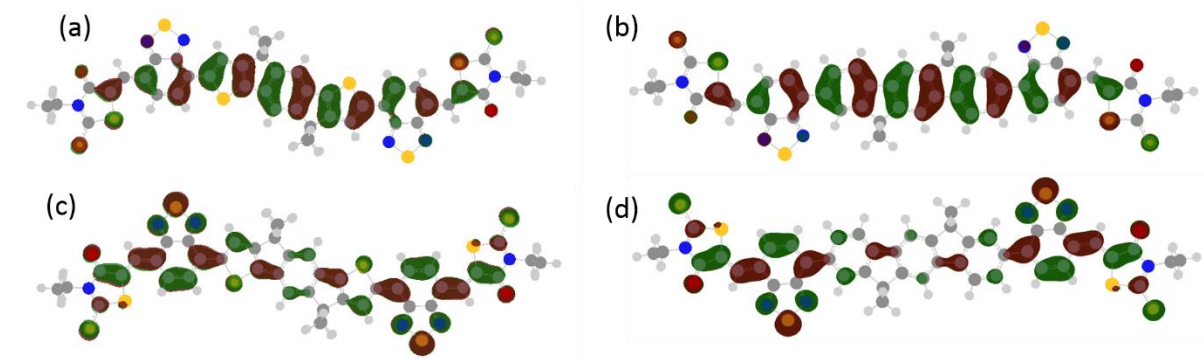

Figure S2. Orbital visualisations at minimised energy structures, simulated using DFT at the B3LYP level of theory with the 6-31G(d,p) basis set. IDTBR HOMO (a) and LUMO (b) are shown with the HOMO (b) and LUMO (d) of IDFBR.

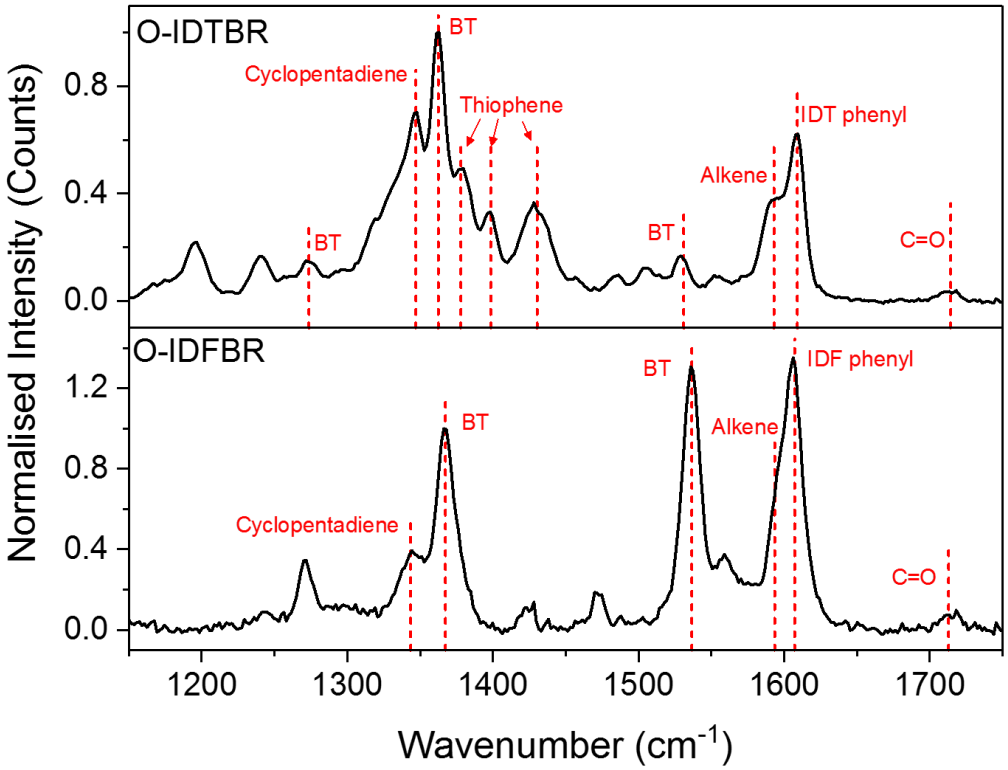

Figure S3.(a) Normalised Raman spectra of O-IDTBR (top) and O-IDFBR (bottom) taken at 457 nm excitation. Peak assignment has been conducted by comparison with the literature and by comparing to the simulated spectra shown in (c) and visualising the associated Raman modes.

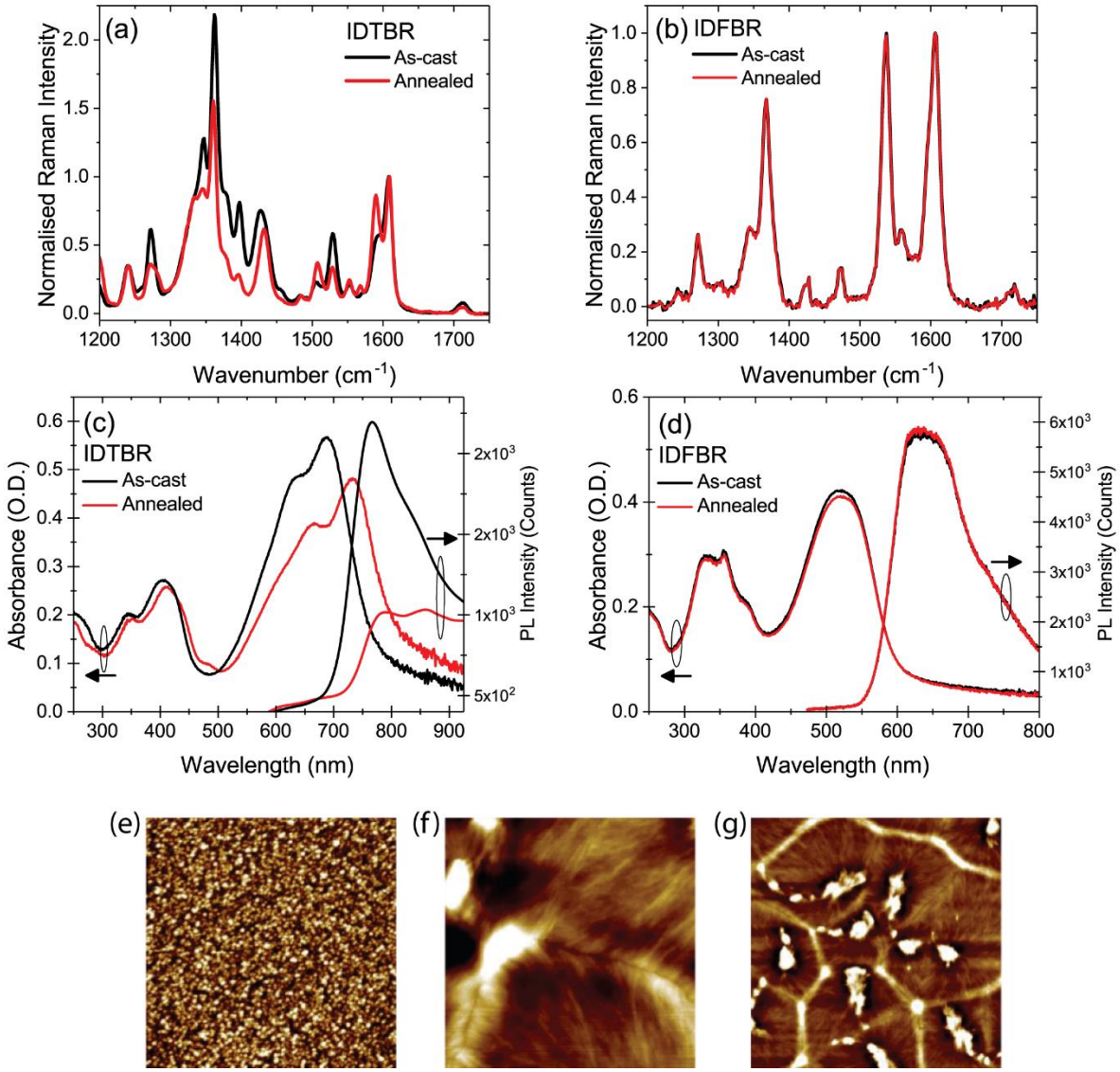

Figure S4. The normalised Raman spectra of IDTBR (a) and IDFBR of as-cast and annealed films (130°C for 10 mins). The absorption and PL spectra at 514 nm excitation of as-cast and annealed films of IDTBR (c) and IDFBR (d). AFM images of as-cast (e) and annealed (f+g) films of O-IDTBR. Annealing conditions are 130°C for 10 minutes in an inert atmosphere. The dimensions of (e+f) are 5x5 µm whilst (g) is 25x25µm.

Neat film annealing

Optimised devices of these acceptors with P3HT are annealed at 130°C for 10 minutes, so the effect of annealing of the neat acceptor films was also investigated.[1,2] IDTBR has a reported recrystallization temperature at ~110°C.[1] Therefore annealing at 130°C leads to an increase in crystallinity forming large crystallite domains (~20 µm, Figure S3), resulting in a red-shift of the lower energy transition by 44 nm and a high scattering background beyond the absorption onset, as well as significant quenching of the photoluminescence (Figure S3 c,d).

This is accompanied by a change in orientation to a more edge-on configuration as seen from the as-cast and annealed film GIWAXS patterns reported in the literature.[1,3] Upon annealing IDTBR there are relative intensity changes to several Raman modes that have large contributions from the *n-octyl* side chains suggesting a reorganisation of these. Other changes include the IDT peak at 1430cm^{-1}, associated with the C-C bonds within the thiophene rings, displaying a clear reduction in FWHM and a shift to higher frequencies. This is indicative of an increase in bond strength, due to increased quinoidal character associated with a more planar conjugated system.[4] Importantly, there is also a reduction in the relative intensity of the three main BT peaks with respect to the phenyl peak at 1609 cm^{-1}, which are indicative of increasing backbone planarity, and discussed more thoroughly in the next section. On the other hand, IDFBR shows no change in properties (Figure S3b,d) upon annealing at this temperature, as is consistent with the lack of phase transitions within this temperature range.[2]

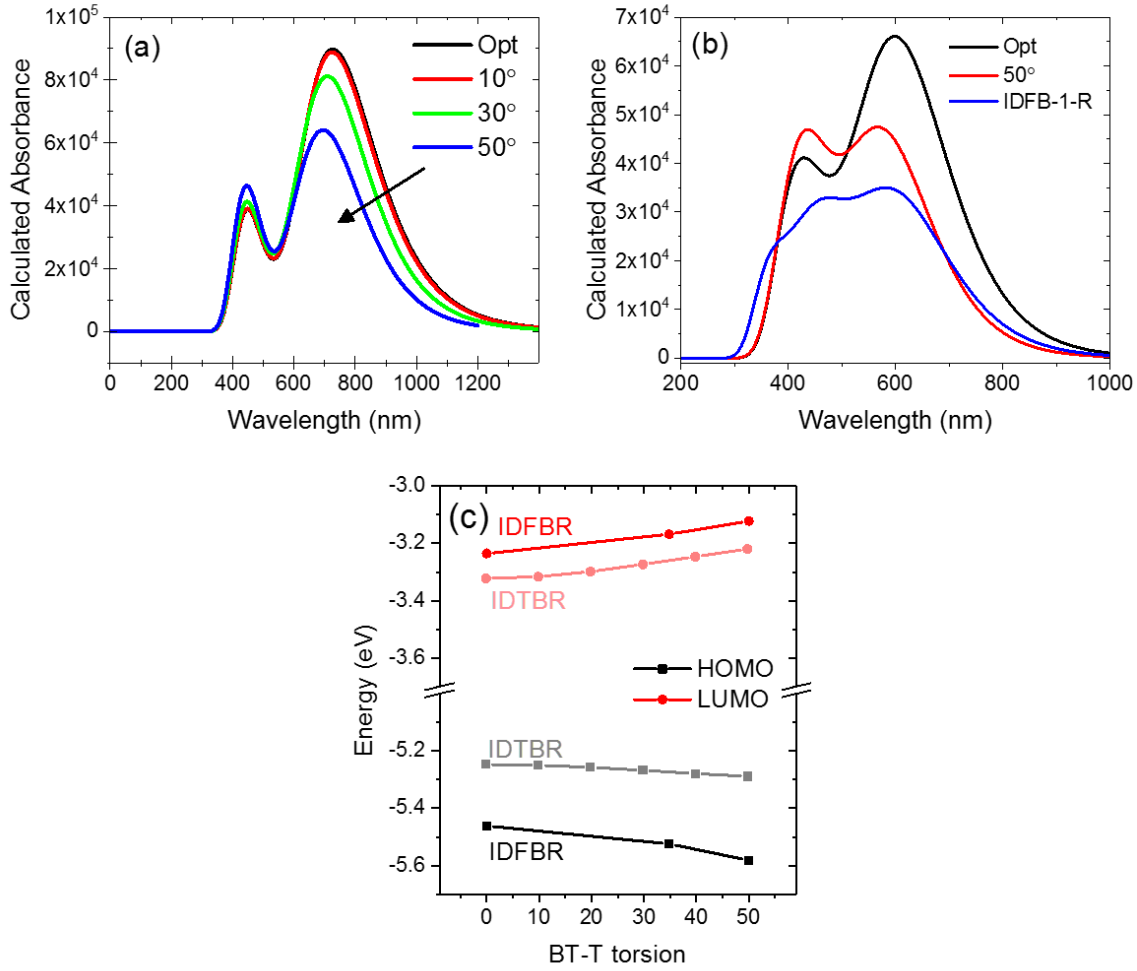

Figure S5. UV/vis spectra simulated using TD-DFT at the B3LYP level of theory with a 6-31G(d,p) basis set. (a) the simulated spectra of IDTBR at different IDT-BT torsion angles, (b) The simulated spectra of IDFBR at the optimised structure (33° IDF-BT dihedral angle), 50° IDF-BT dihedral angle, and with a loss of one rhoadanine group, replaced by a capping hydrogen atom. (c) The calculated energy levels of IDTBR and IDFBR single molecules in the gas-phase at different Core-BT dihedral angles.

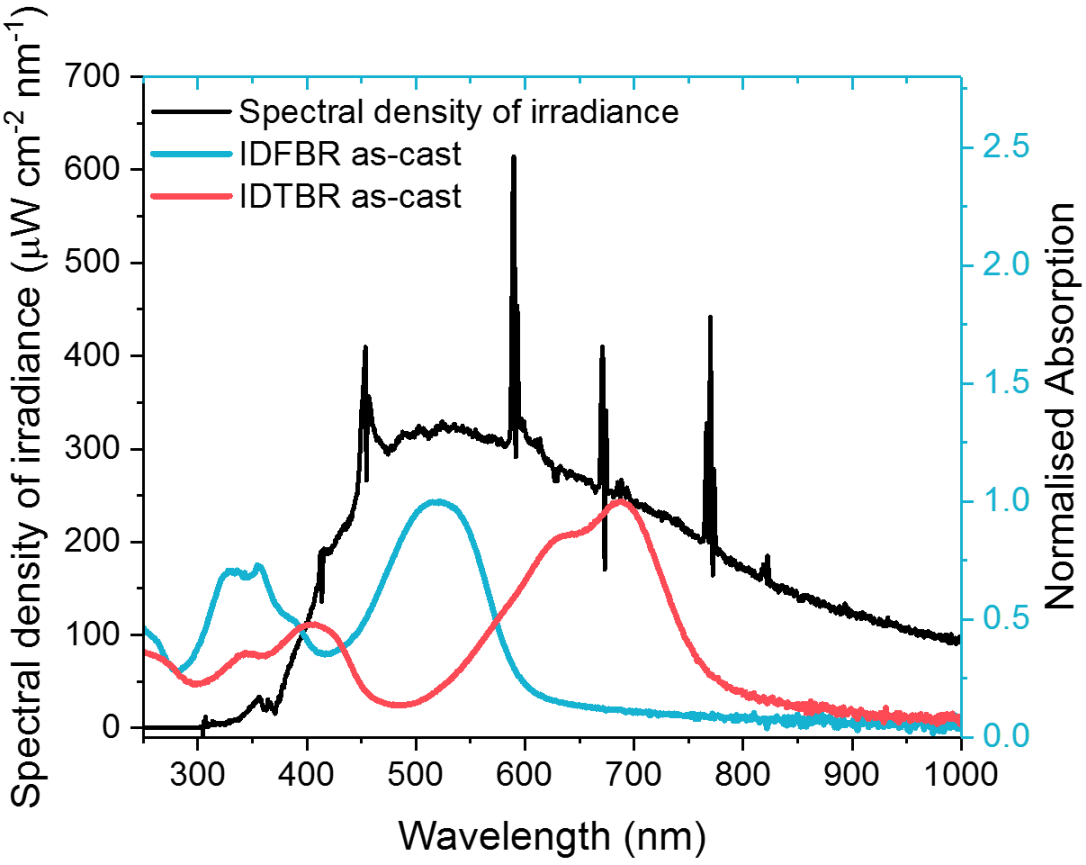

Figure S6. Spectrum of the Solixon A-20 solar simulator used for degradation, and the normalised absorption spectra of as-cast IDTBR and IDFBR films. Note the relatively small emission between 300-400 nm.

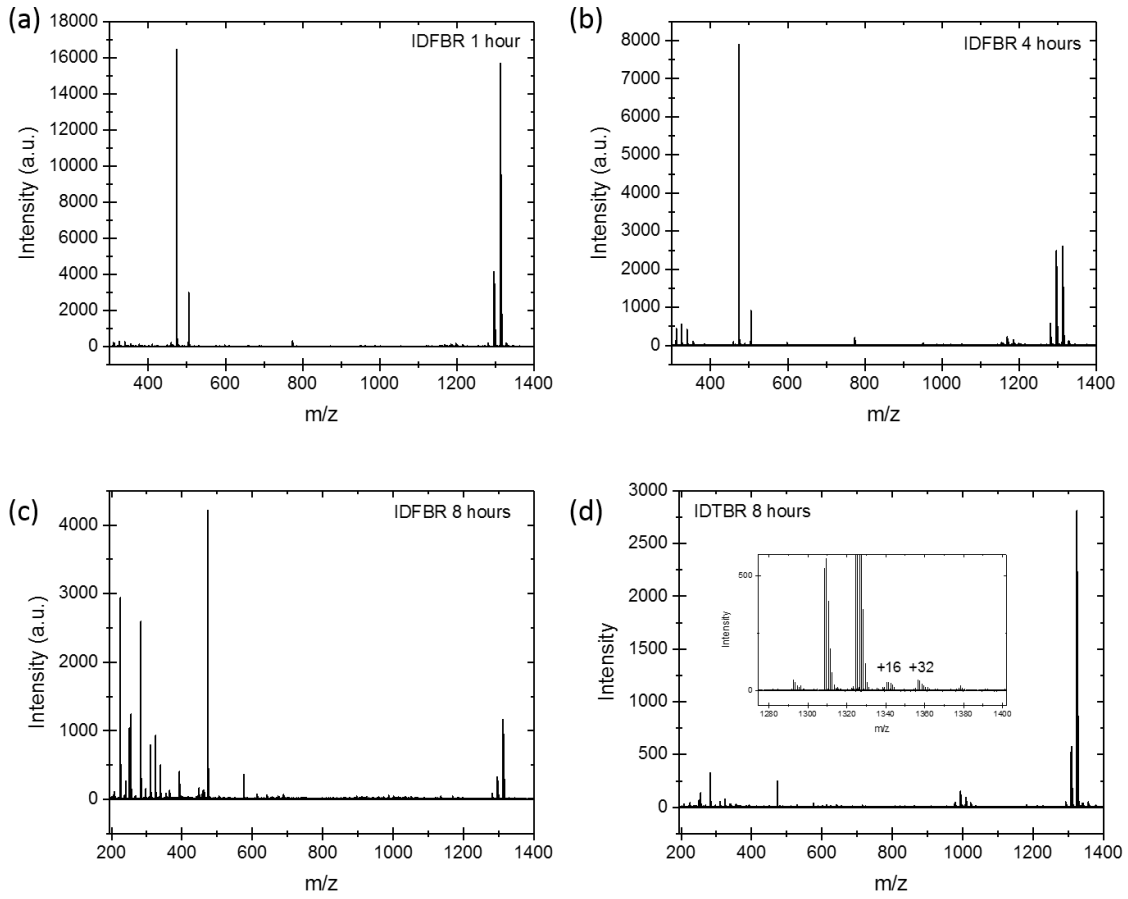

Figure S7. Mass spectra of IDFBR, degraded as films at different degradation times, 1 hour (a), 4 hours (b) and 8 hours (c). (d) the mass spectrum of degraded IDTBR after 8 hours of degradation, the inset shows a zoomed in region near the molecular ion peak, showing the addition of oxygen.

Experimental procedure for mass spectroscopy

Samples for mass spectrometry were prepared in chlorobenzene at an approximate concentration of 1 mg mL^{-1}. MALDI matrix anthracene was purchased from Sigma-Aldrich Company Ltd. (Gillingham, UK), and dissolved in chlorobenzene at 10 mg mL^{-1}. Solutions of sample and matrix were mixed together so the matrix was in 250–1000 fold molar excess, typically 1 μL of sample to 49 μL of matrix. 0.5 μL of each of these mixture solutions for each sample was spotted onto the MALDI plate and dried in air. MALDI-TOF spectra were acquired in negative-reflectron mode using an ultrafleXtreme mass spectrometer (Bruker Daltonics, Bremen, Germany), which is equipped with a Smartbeam-II Nd:YAG laser (λ= 355 nm); sample ions were observed as negative radical species ($M^{-\bullet}$). Data was acquired using flexControl software v3.4, while post-acquisition processing of data was performed by flexAnalysis software v3.4.

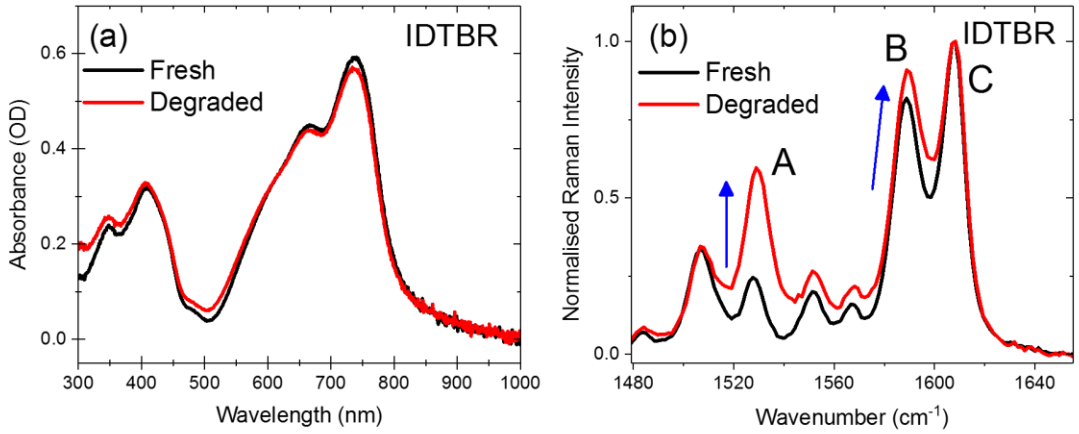

Figure S8. (a) Absorption spectra of annealed O-IDTBR before and after 8 hours of solar simulator degradation in air. Note only minor bleaching of low energy peak. (b) Raman spectra of annealed O-IDTBR before and after 8 hours of solar simulator degradation in air, 488 nm excitation laser. Upon degradation the same key peak changes are observed as in the as-cast films.

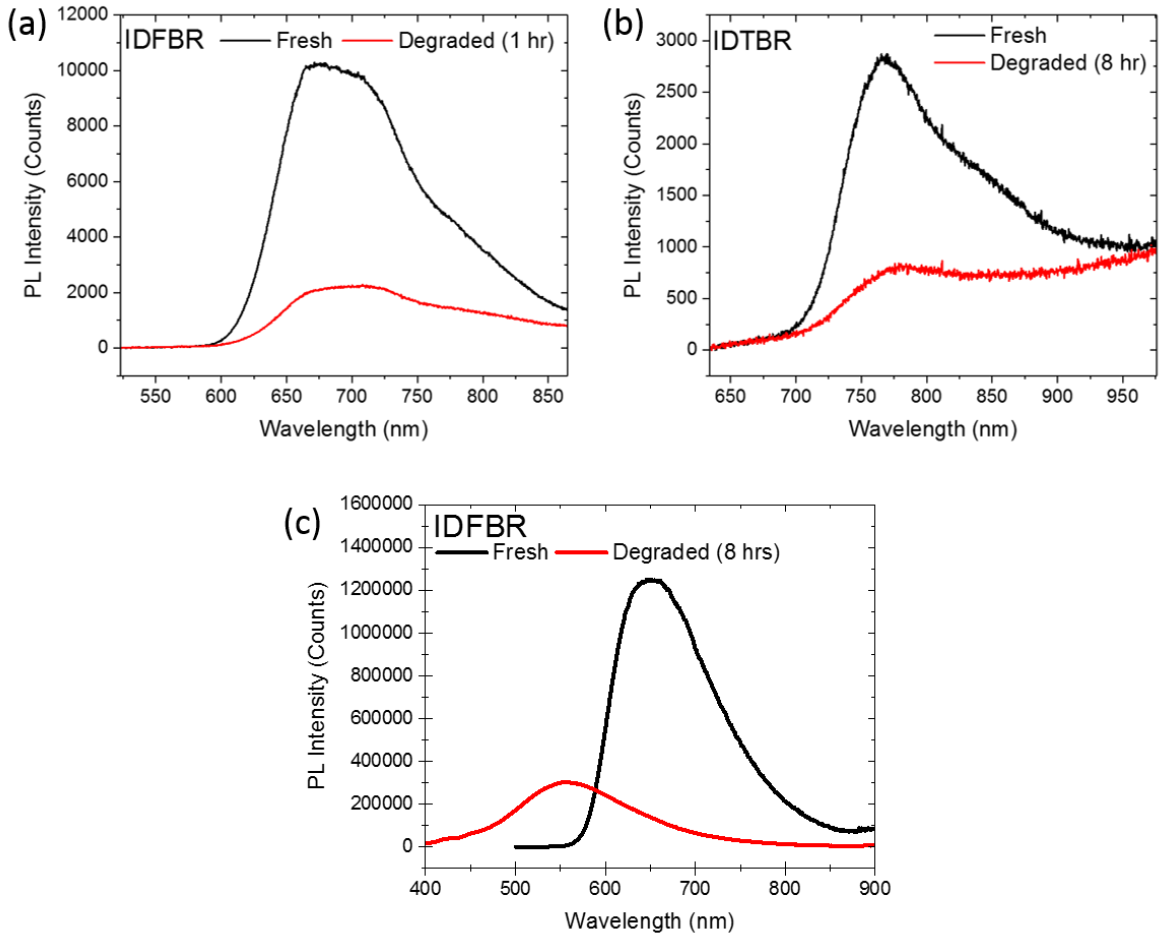

Figure S7. Photoluminescence spectra of fresh and degraded IDFBR (a) and IDTBR (b) thin films, obtained at 514 nm excitation using the Raman set-up described in the main text. (c) the PL spectra of fresh and heavily degraded IDFBR thin films taken using an Edingburgh Instruments FLS1000 PL Spectrometer, the fresh spectrum was taken at 405 nm excitation whilst the degraded spectrum were taken at 350 nm excitation.

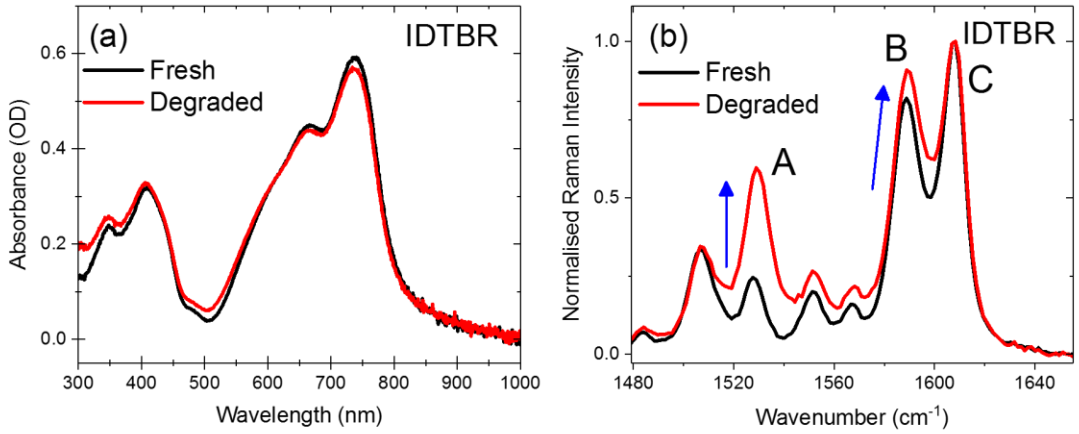

Figure S8. (a) Absorption spectra of annealed O-IDTBR before and after 8 hours of solar simulator degradation in air. Note only minor bleaching of low energy peak. (b) Raman spectra of annealed O-IDTBR before and after 8 hours of solar simulator degradation in air, 488 nm excitation laser. Upon degradation the same key peak changes are observed as in the as-cast films.

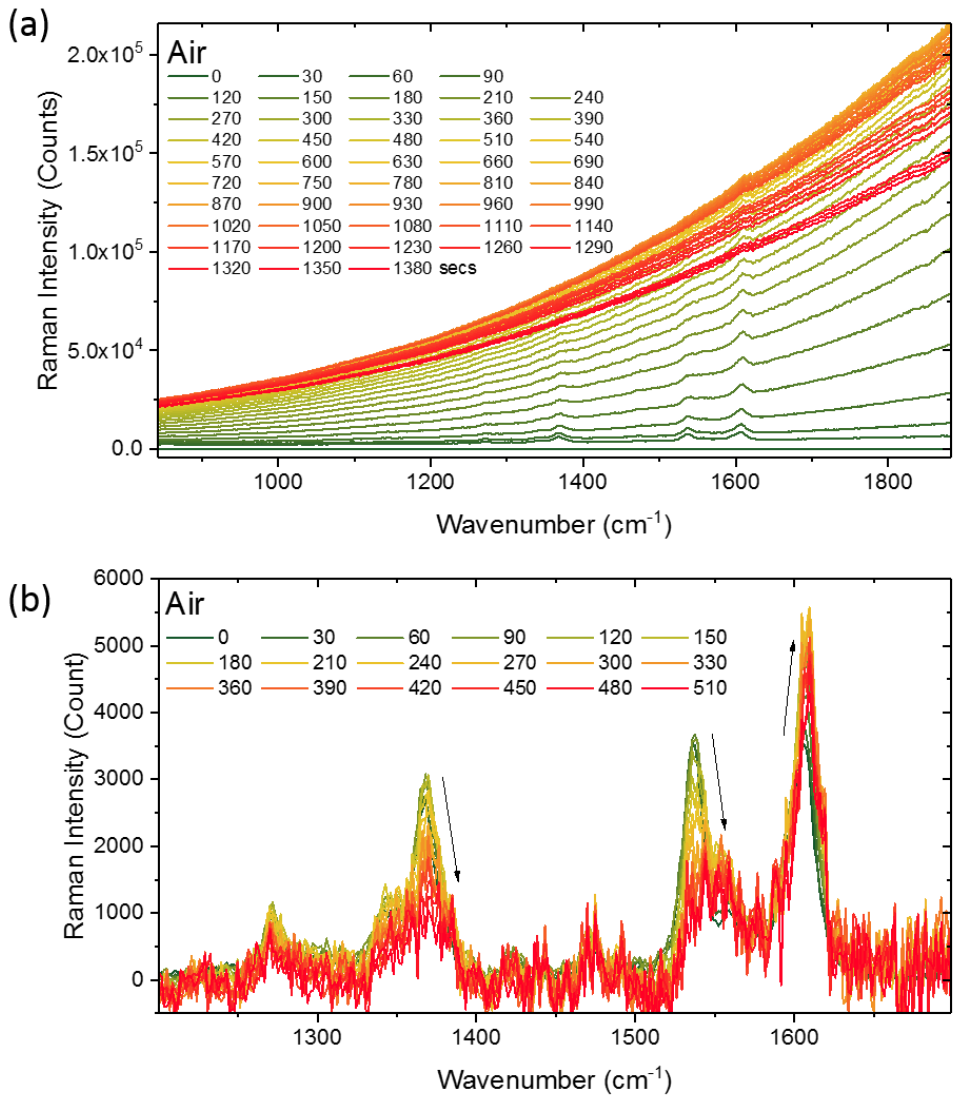

Figure S9. (a) Raw in situ Raman spectra of IDFBR taken at 457 nm excitation in air. (b) baseline corrected spectra at different times taken from the spectra shown in (a).

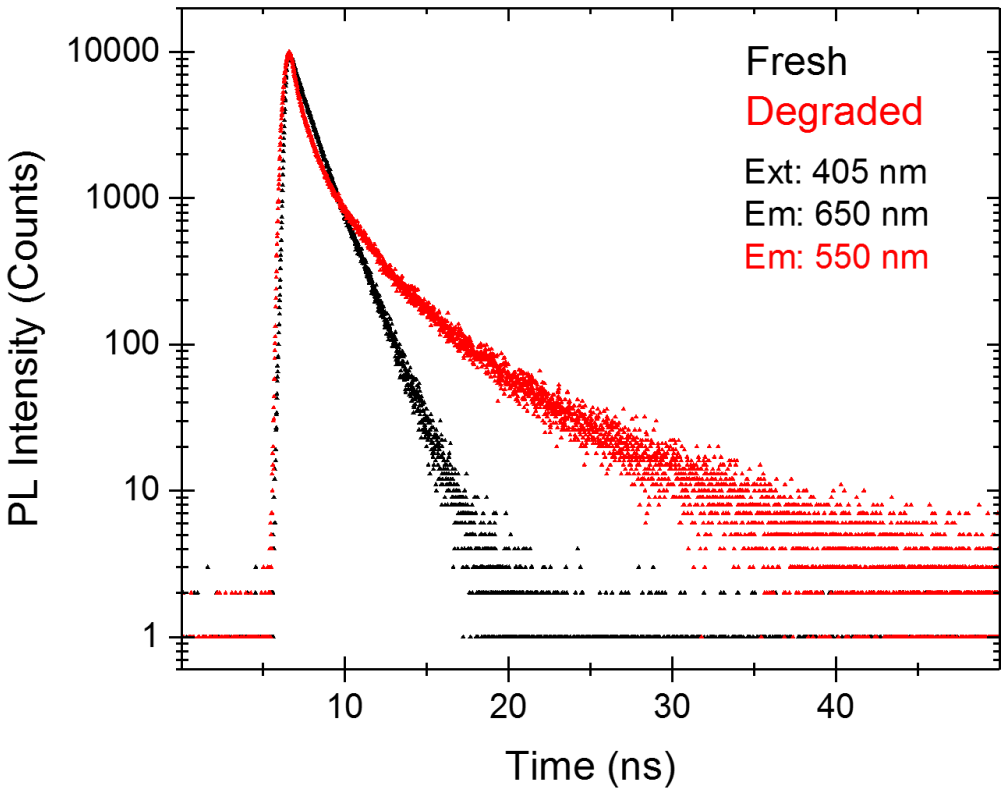

Figure S10.PL transients measured by time correlated single photon countingmeasurements. Spectra show the decay of PL of the fresh and heavily degraded (8 hour) IDFBR films, taken at 405 nm excitation and probed at the PL maxima of 650 and 550 nm for the fresh and degraded films respectively.

Experimental procedure for TCSPC Spectroscopy

Time-correlated-single-photon-counting spectroscopy was carried out using an Edinburgh Instruments FLS1000 spectrometer. The excitation source was a 405 nm picosecond pulsed diode laser. Fitting was carried out using Edinburgh Photonics FAST software, using a reconvolution fit with the instrument response function.

Discussion of TCSPC results

The decay of the high energy PL at 550 nm emission can be fitted using three exponential decay components with time constants of 0.25, 1.53 and 5.67 ns and corresponding fractions of 35.6%, 42.7% and 21.7% respectively, whereas the decay of the fresh PL at 650 nm is bi-exponential, but dominated by a single exponential process, with time constants of 1.2 and 2.3 ns and fractions of 93.4% and 6.6%. The different decay processes indicate that the emissive species are distinct.

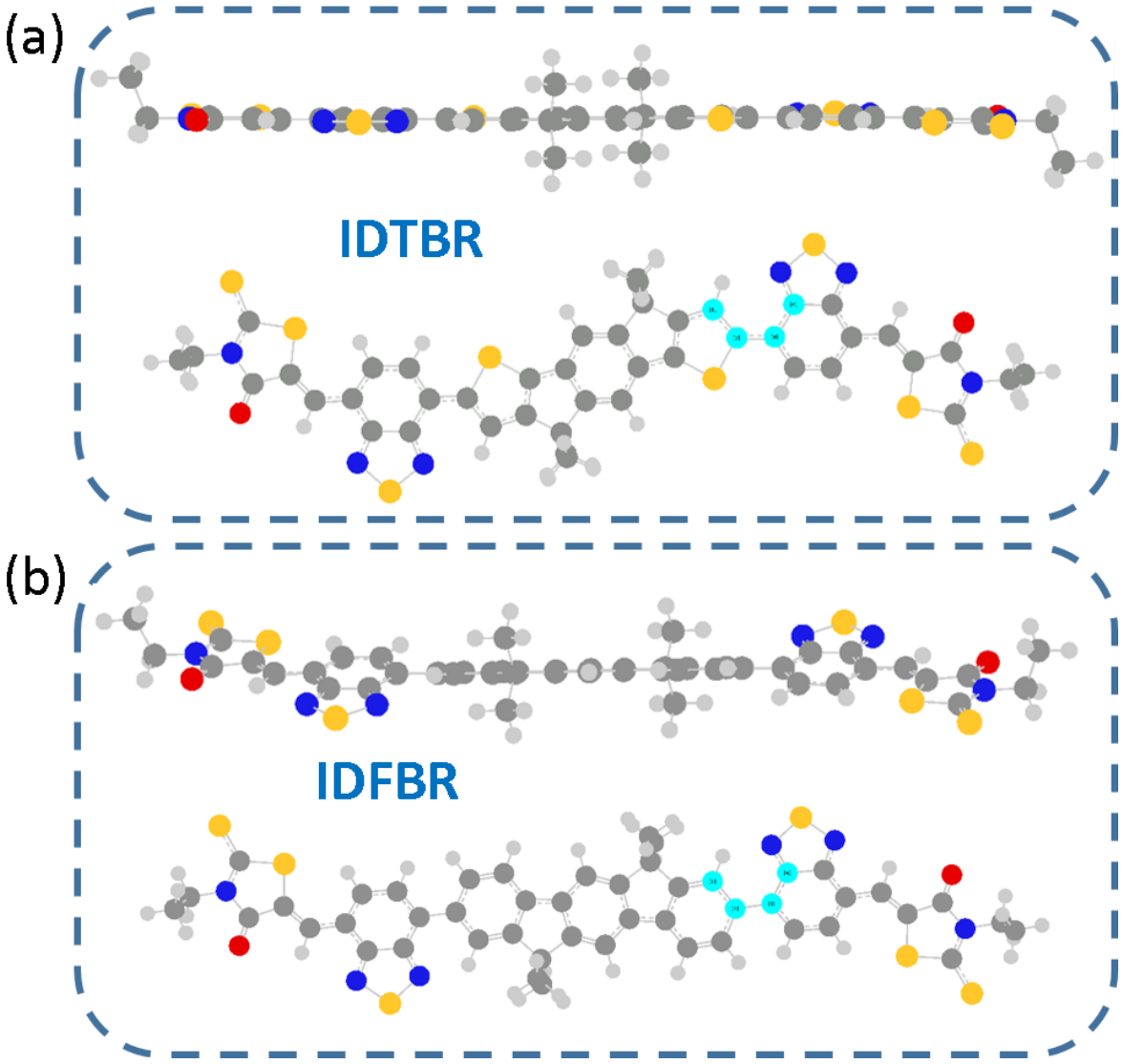

Figure 11. TD-DFT optimised geometries of the first excited state of IDTBR (a) and IDFBR (b) using B3LYP and a basis set of 631G(d,p). The average of the two core-BT dihedral angles is shown in Table 1, below. There is an increase in planarity upon excitation for both molecules.

Table 1. Core-BT dihedral angles of optimised structures of the S_0 and S_1 states of IDTBR and IDFBR. TD-DFT simulations using the B3LYP level of theory, with a 6-31G(d,p) basis set.

Molecule	S_0 Core –BT Dihedral	S_1 Core-BT Dihedral
IDTBR	2.13°	0.35°
IDFBR	34.8°	25.7°

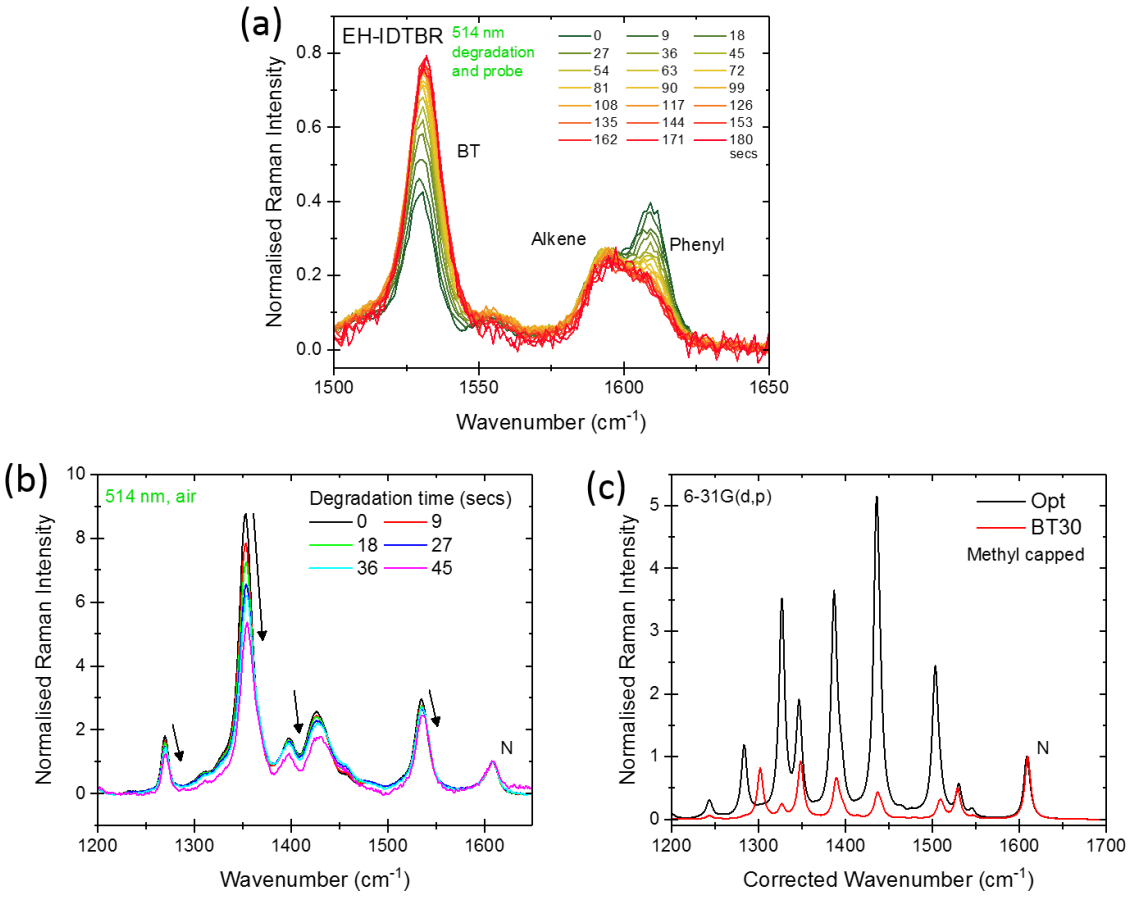

Figure S12. Normalised in situ Raman spectra during laser degradation of EH-IDTBR (a) and the polymer IDTBT (b) in air, taken at 514 nm excitation. (c) The DFT simulated Raman spectra of an IDTBT pentamer at the B3LYP level of theory with a 6-31G(d,p) basis set. Two normalised spectra are shown, the planar optimised geometry and at a fixed IDT-BT dihedral angle of 30°.

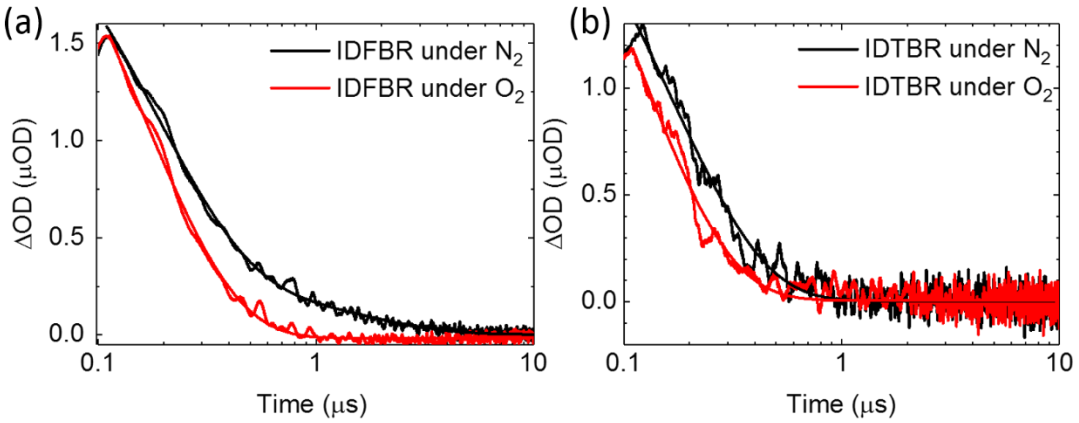

Figure S13. Transient absorption spectra as a function of time for neat IDFBR (b) and IDTBR (a), showing the effect of oxygenn quenching on lifetime, note that the quenching is more pronounced and the lifetime longer for IDFBR.

Experimental procedure for transient absorption measurements

Microsecond transient absorption kinetics were measured using laser excitation pulses (<10 ns) generated from a tuneable optical parametric oscillator (Opolette 355). Samples were probed using the light output of a tungsten lamp and signals were recorded with Si and InGaAs photodiodes, housed in a preamplifier and an electronic filter (Costronics Electronics) connected to a dual channel oscilloscope and PC. Probe wavelengths were selected with a monochromator.

Discussion of transient absorption measurements

To investigate the interaction with oxygen we use microsecond transient absorption measurements to probe the excited states of the materials. Films of neat IDFBR and IDTBR, probed at the photo-induced maxima, exhibited oxygen-sensitive bi-exponential decays (Figure S10). This can be assigned to triplet exciton $T_1 \rightarrow T_n$ absorption. These triplet excitons are most likely formed via direct intersystem crossing from the singlet excitons and quenched by triplet ground state oxygen, forming singlet oxygen as previously observed for polymers and fullerene acceptors.[5,6]

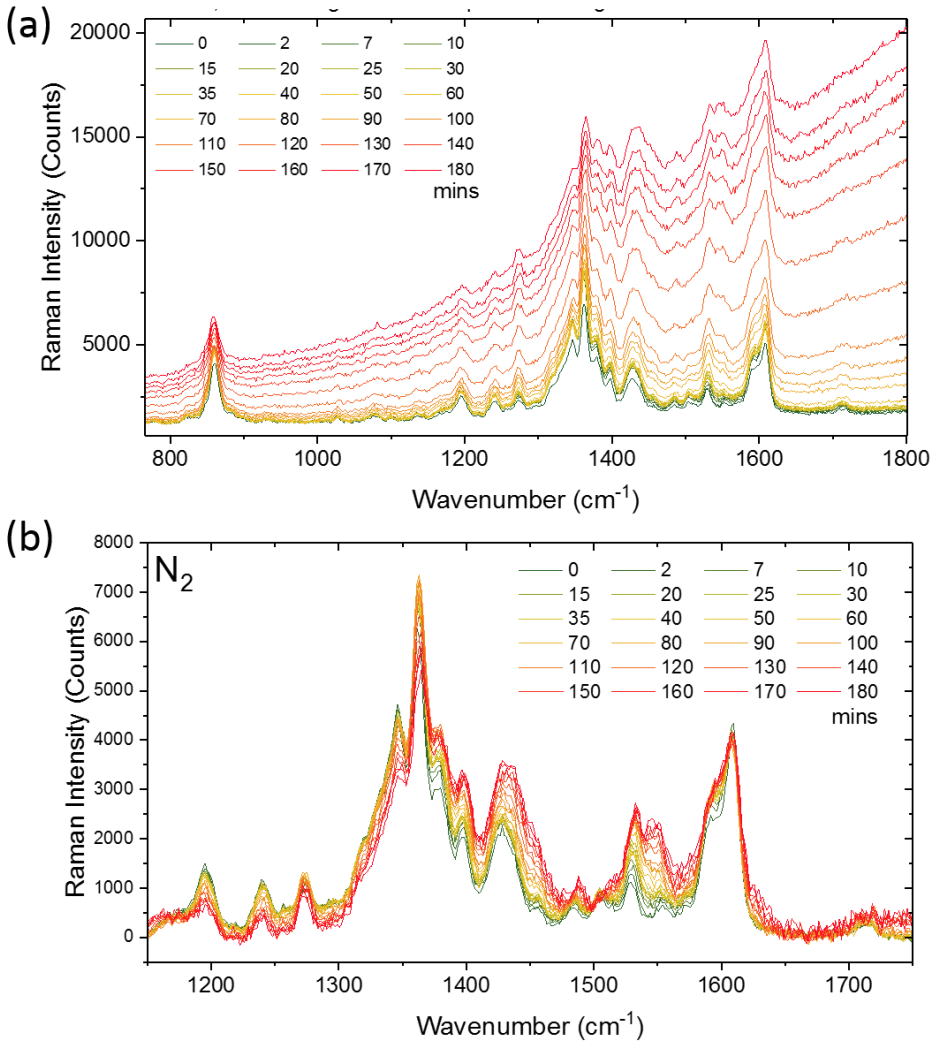

Figure S14. (a) Raw in situ Raman spectra of IDTBR taken at 457 nm excitation under a flow of nitrogen. (b) baseline corrected spectra at different times taken from the spectra shown in (a).

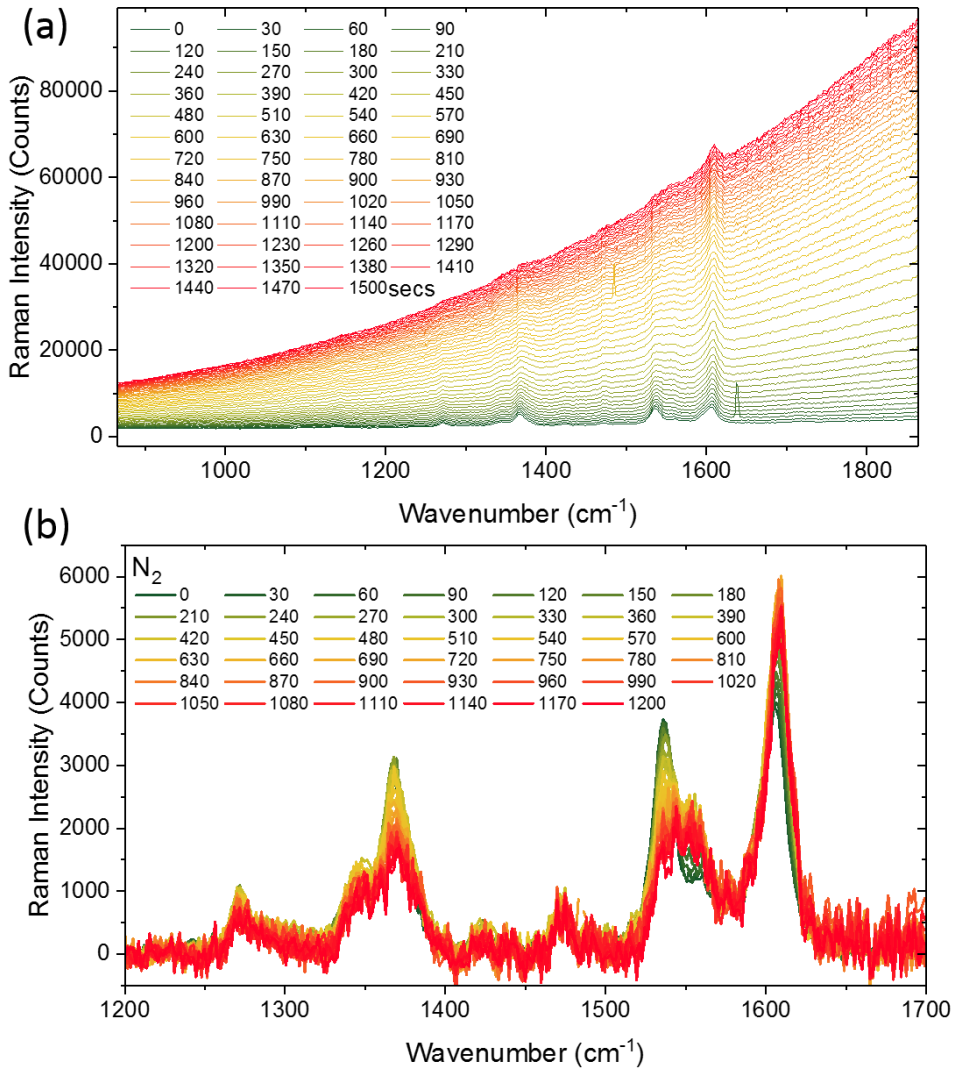

Figure S15. (a) Raw in situ Raman spectra of IDFBR taken at 457 nm excitation under a flow of nitrogen. (b) baseline corrected spectra at different times taken from the spectra shown in (a).

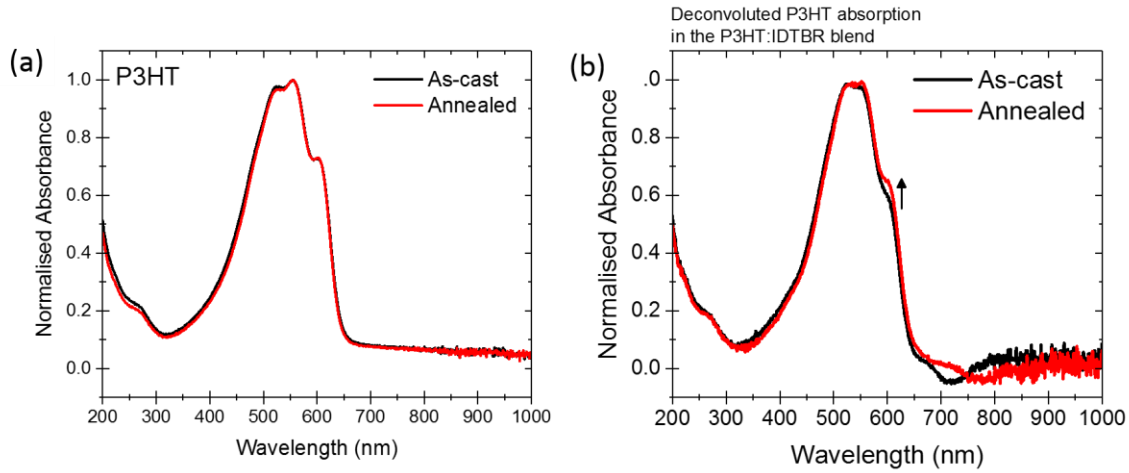

Figure S16. UV/vis absorption spectra of as cast and annealed P3HT (a) and P3HT:IDTBR (b) with the IDTBR absorption substracted to investigate the change in P3HT crsyatllinity upon annealing. Annealing conditions: 130°C for 10 minutes in N_2.

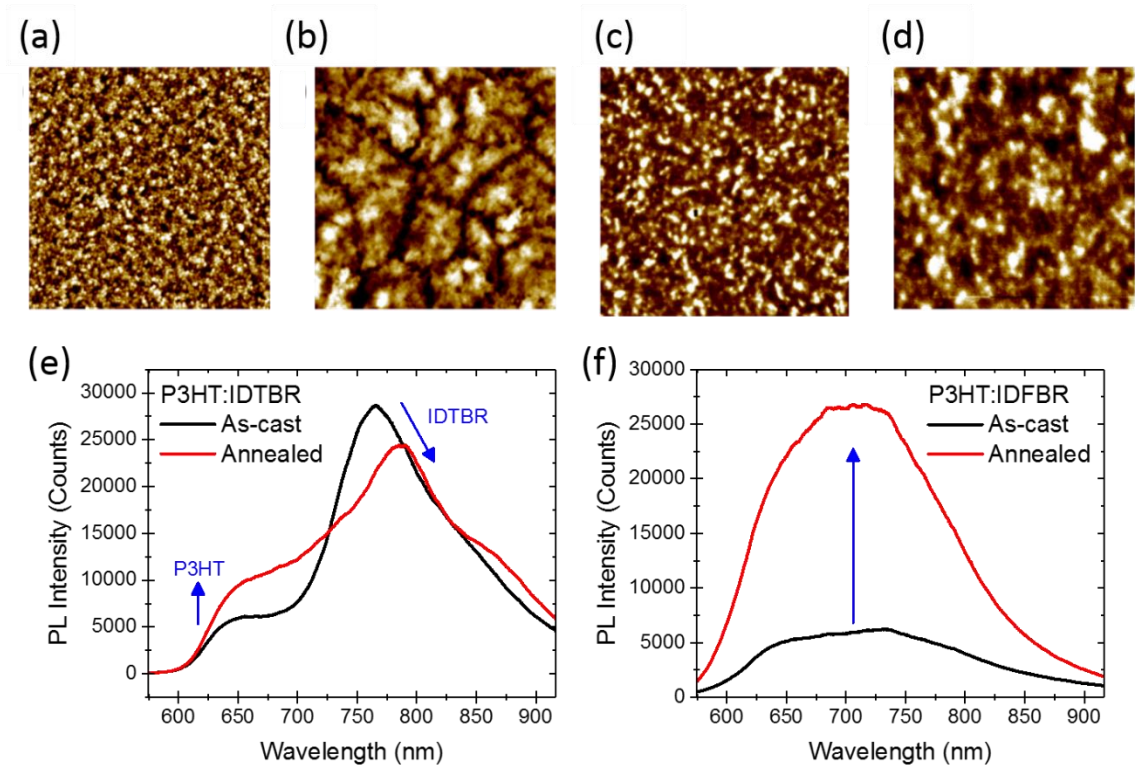

Figure S17. AFM images with the dimensions 5 x 5 µm of as-cast P3HT:IDTBR (a), as-cast P3HT:IDFBR (c), annealed P3HT:IDTBR (b) and annealed P3HT:IDFBR (d). PL spectra taken using the Raman set-up described in the main text, at 514 nm excitation of the as-cast and annealed films of P3HT:IDTBR (e) and P3HT:IDFBR (f). Annealing conditions: 130°C for 10 minutes in N_2.

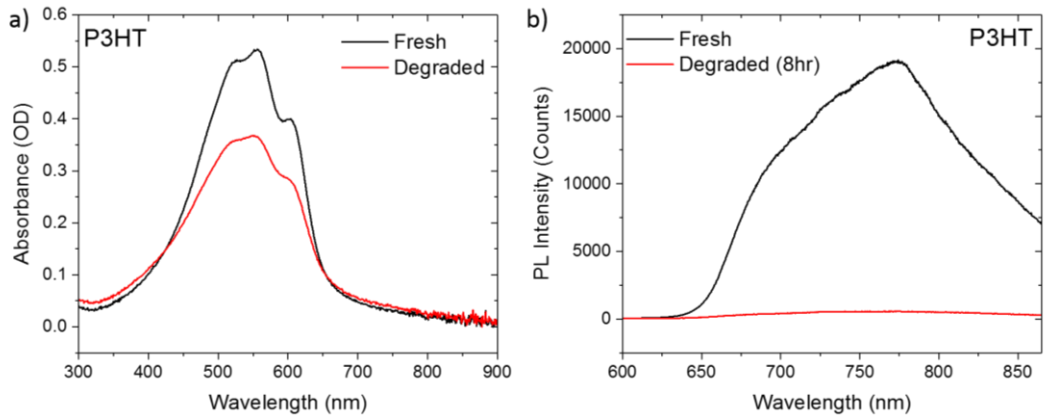

Figure S18. (a) UV/vis absorption spectra of fresh annealed P3HT films and films degraded for 8 hours using a solar simulator in air. (b) PL spectra of the same films, taken at 514 nm excitation using the Raman set-up descirbed in the main text.

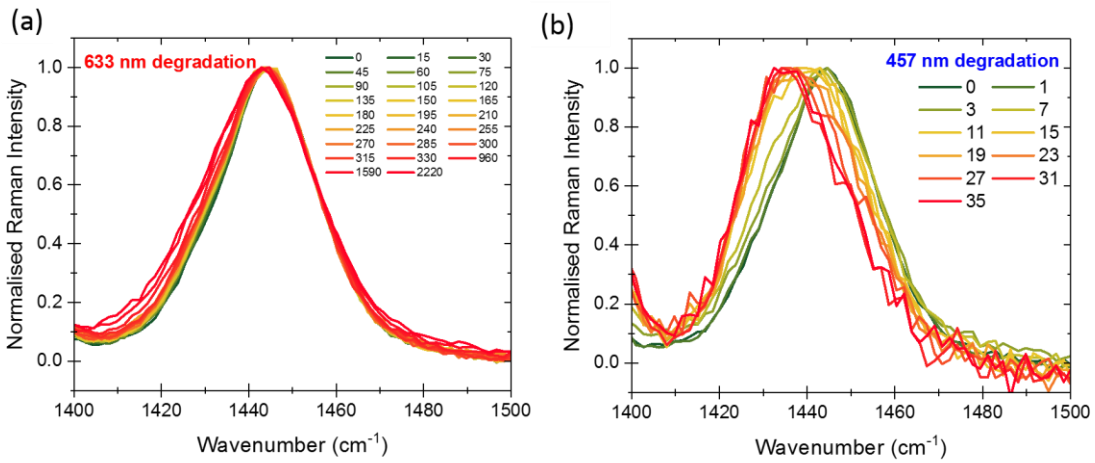

Figure S19. Normalised in situ Raman spectra of the P3HT:IDTBR blend using a 633 nm probe. The degradation sources used were 633 nm (a) and 457 nm (b). The peak shown and normalised to is the P3HT C=C peak.

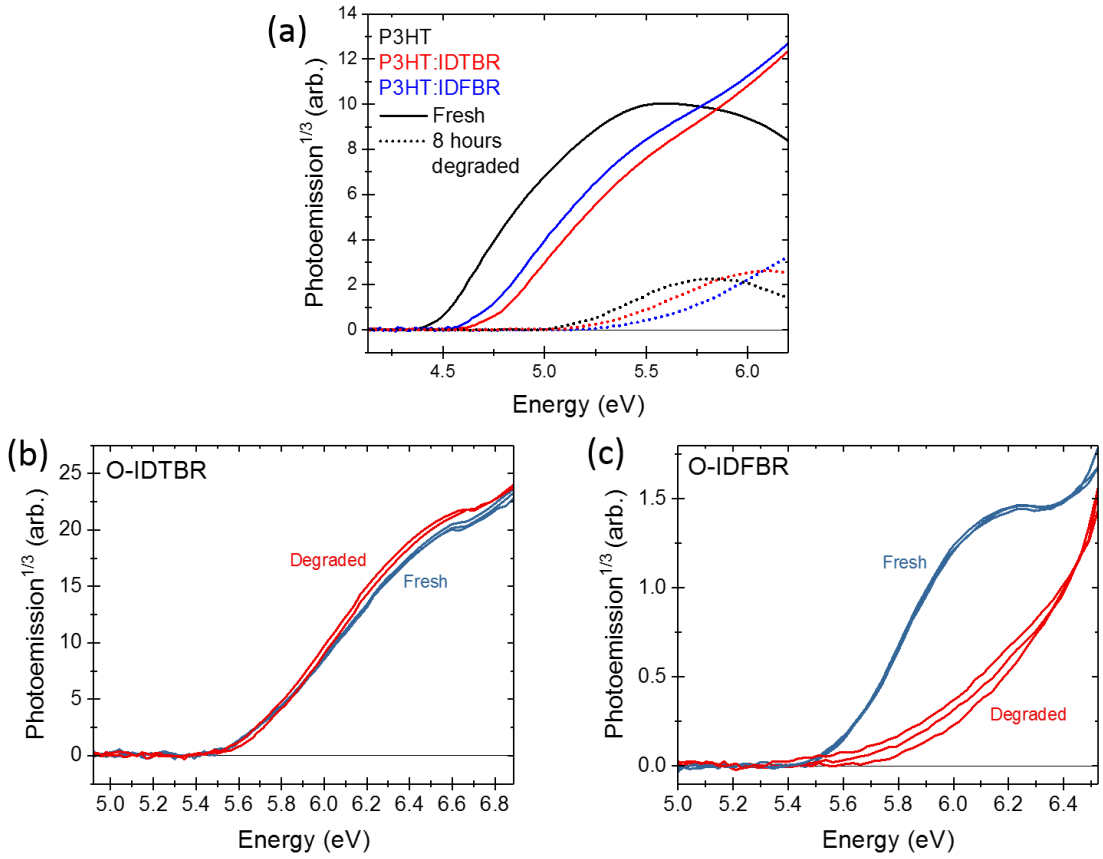

Figure S20. Air photoemission spectra of thin films on an ITO substrate of fresh and degraded P3HT, P3HT:IDTBR and P3HT:IDFBR (a), IDTBR (b) and IDFBR (c). Degradation was conducted for 8 hours under 1 sun illumination in air. The HOMO level is taken by fitting a linear line to the cube root of emission (plotted) and finding the intercept.

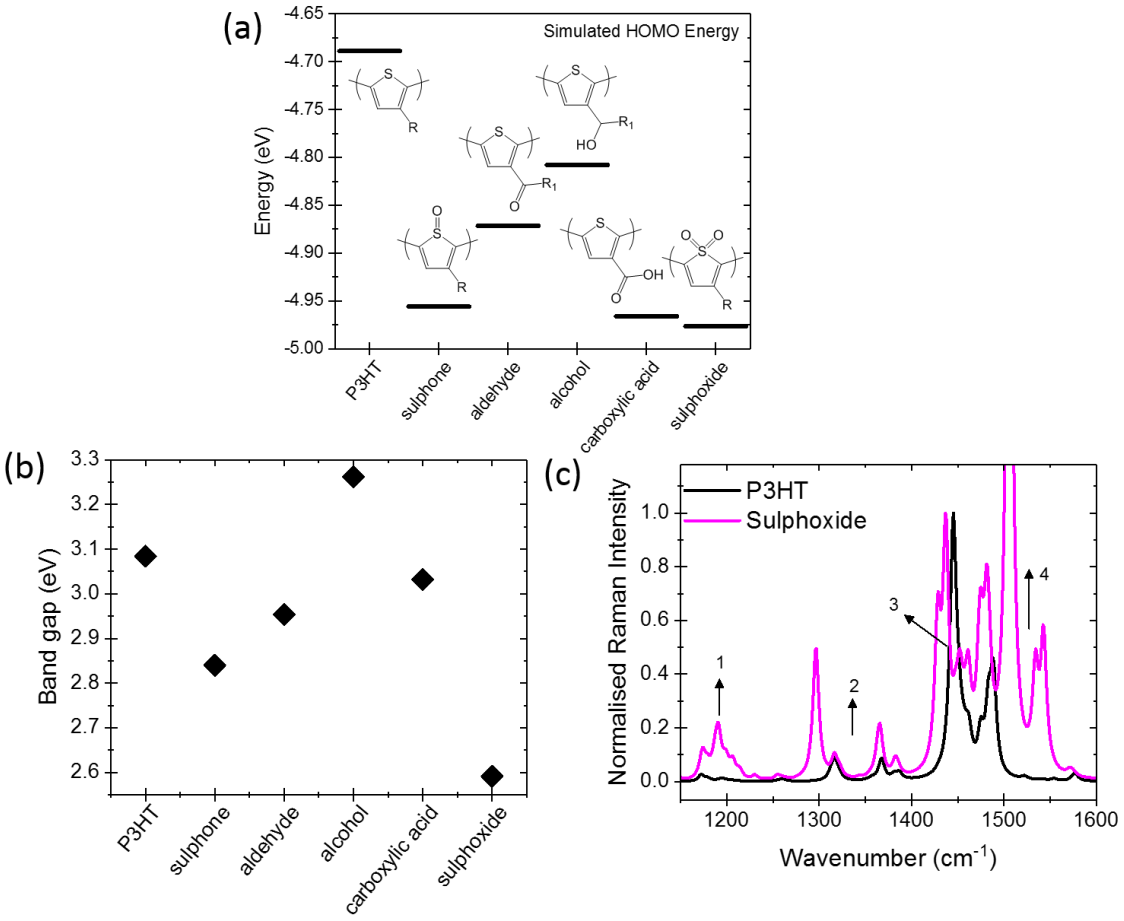

Figure S21. (a) Simulated HOMO levels of P3HT pentamers with different potential oxidation products on the central monomer as shown in the inset chemical structures. (b) Simulated band gap of several potential oxidation products of P3HT. (c) Simulated Raman spectra of P3HT and a P3HT pentamer with oxidation of the central thiophene unit to create a sulphoxide group. DFT simulations were carried out on pentamers with ethyl-side chains, with the central unt being oxidised. Calculations were carried out at the B3LYP level of theory with a 6-31G(d,p) basis set.

Additional Discussion

The calculated Raman spectra of a P3HT pentamer with and without a sulphoxide group on the central thiophene unit is shown in Figure S20c. It should be noted that after degradation the Raman spectra will contain contributions from both the fresh and degraded P3HT, so a Raman spectra matching that of the oxidised oligomer will not be replicated experimentally. However, there are some clear similarities between the calculated and experimental spectra (main text, Figure 7c). There is an increase in the relative intensity of the peaks labelled 1 and 4 at *ca.* 1200 and 1525 cm^{-1} similar to that observed experimentally. The general broadening of the main feature to lower frequency experimentally may be due to the shift of the main C=C peak to lower frequencies labelled 3 in the calculated spectra. The peaks labelled 2 may also be contributing to this broadening.

Supporting Information References

[1] S. Holliday, R. S. Ashraf, A. Wadsworth, D. Baran, S. A. Yousaf, C. B. Nielsen, C.-H. Tan, S. D. Dimitrov, Z. Shang, N. Gasparini, M. Alamoudi, F. Laquai, C. J. Brabec, A. Salleo, J. R. Durrant, I. McCulloch, *Nat. Commun.* **2016**, *7:11585*, DOI 10.1038/ncomms11585.

[2] D. Baran, R. A. S. Ashraf, D. A. Hanifi, M. Abdelsamie, N. Gasparini, J. A. Röhr, S. Holliday, A. Wadsworth, S. Lockett, M. Neophytou, C. J. M. Emmott, J. Nelson, C. J. Brabec, A. Amassian, T. Kirchartz, J. R. Durrant, I. Mcculloch, D. Baran, R. A. S. Ashraf, S. Holliday, A. Wadsworth, S. Lockett, P. J. R. Durrant, *Nat. Mater.* **2016**, *16*, 363.

[3] S. Badgujar, C. E. Song, S. Oh, W. S. Shin, S.-J. Moon, J.-C. Lee, I. H. Jung, S. K. Lee, *J. Mater. Chem. A* **2016**, *4*, 16335.

[4] W. C. Tsoi, D. T. James, J. S. Kim, P. G. Nicholson, C. E. Murphy, D. D. C. Bradley, J. Nelson, J. S. Kim, *J. Am. Chem. Soc.* **2011**, *133*, 9834.

[5] E. M. Speller, J. D. McGettrick, B. Rice, A. M. Telford, H. K. H. Lee, C. H. Tan, C. S. De Castro, M. L. Davies, T. M. Watson, J. Nelson, J. R. Durrant, Z. Li, W. C. Tsoi, *ACS Appl. Mater. Interfaces* **2017**, *9*, 22739.

[6] Y. W. Soon, S. Shoaee, R. S. Ashraf, H. Bronstein, B. C. Schroeder, W. Zhang, Z. Fei, M. Heeney, I. McCulloch, J. R. Durrant, *Adv. Funct. Mater.* **2014**, *24*, 1474.